Modeling of craton stability using a viscoelastic rheology

Marcus J. Beuchert,[1,2] Yuri Y. Podladchikov,[1] Nina S. C. Simon,[1] and Lars H. Rüpke[3]

Received 24 March 2009; revised 18 April 2010; accepted 3 August 2010; published 25 November 2010.

[1] Archean cratons belong to the most remarkable features of our planet since they represent continental crust that has avoided reworking for several billions of years. Even more, it has become evident from both geophysical and petrological studies that cratons exhibit deep lithospheric keels which equally remained stable ever since the formation of the cratons in the Archean. Dating of inclusions in diamonds from kimberlite pipes gives Archean ages, suggesting that the Archean lithosphere must have been cold soon after its formation in the Archean (in order to allow for the existence of diamonds) and must have stayed in that state ever since. Yet, although strong evidence for the thermal stability of Archean cratonic lithosphere for billions of years is provided by diamond dating, the long-term thermal stability of cratonic keels was questioned on the basis of numerical modeling results. We devised a viscoelastic mantle convection model for exploring cratonic stability in the stagnant lid regime. Our modeling results indicate that within the limitations of the stagnant lid approach, the application of a sufficiently high temperature-dependent viscosity ratio can provide for thermal craton stability for billions of years. The comparison between simulations with viscous and viscoelastic rheology indicates no significant influence of elasticity on craton stability. Yet, a viscoelastic rheology provides a physical transition from viscously to elastically dominated regimes within the keel, thus rendering introduction of arbitrary viscosity cutoffs, as employed in viscous models, unnecessary.

Citation: Beuchert, M. J., Y. Y. Podladchikov, N. S. C. Simon, and L. H. Rüpke (2010), Modeling of craton stability using a viscoelastic rheology, *J. Geophys. Res.*, *115*, B11413, doi:10.1029/2009JB006482.

1. Introduction

1.1. Constraints on Ages and Geotherms of Archean Cratons

[2] The most ancient part of many continents consists of Archean crust, which forms Archean cratons. It has long been recognized that the occurrence of diamond bearing kimberlite pipes is restricted to these Archean cratons [*Levinson et al.*, 1992], a relation referred to as "Clifford's rule" [*Janse and Sheahan*, 1995], which suggests that the diamonds also might have formed in the Archean. This was confirmed by the first isotopic dating of inclusions extracted from South African diamonds [*Kramers*, 1979; *Richardson et al.*, 1984]. *Richardson et al.* [1984] obtained Archean Sm-Nd isotope model ages from garnets and clinopyroxenes. The analyses of radiogenic isotopes (Rb-Sr, Sm-Nd and U-Pb) on mantle xenoliths from kimberlites also suggested that cratonic mantle keels are ancient, but they also showed that the mantle has been affected by various types of metasomatism since the Archean [*Boyd et al.*, 1985; *Carlson et al.*, 1999; *Griffin et al.*, 1999; *Kramers et al.*, 1983; *Menzies and Murthy*, 1980; *O'Reilly and Griffin*, 1996]. However, these metasomatic events might be localized along melt or fluid pathways and do not seem to have destroyed the keel [*Carlson et al.*, 1999; *Malkovets et al.*, 2007; *Pearson et al.*, 2002; *Simon et al.*, 2007].

[3] The problem with most radiogenic isotope systems is that they are formed by incompatible elements that have very low concentrations in refractory mantle, but are strongly concentrated in melts and fluids. Mantle metasomatism therefore easily disrupts these systems and they are not well suited to date the original formation of the cratonic keel [*Carlson et al.*, 1999; *Walker et al.*, 1989]. Large progress in dating the main melt extraction event that affected mantle that now forms cratonic keels was therefore made when the Re-Os technique became available. Os is compatible during mantle melting and therefore concentrates in the mantle residue, whereas Re is almost quantitatively extracted with the melt at large degrees of melting [*Walker et al.*, 1989]. Re-Os ages on kimberlite borne mantle xenoliths have a strong mean in the late Archean [*Carlson et al.*, 1999; *Griffin et al.*, 2003; *Pearson et al.*, 2002]. Where the lithospheric mantle has been largely replaced by a major tectonic or magmatic event, as for example underneath the South African Premier mine during the 2 Ga Bushveld intrusion, Re-Os ages reflect these disruptions [*Carlson et al.*, 1999]. It has been shown that some

[1]Physics of Geological Processes, University of Oslo, Oslo, Norway.
[2]Now at Institut für Geowissenschaften, Facheinheit Geophysik, Goethe-Universität Frankfurt, Frankfurt am Main, Germany.
[3]Future Ocean, IFM-GEOMAR, Kiel, Germany.

0148-0227/10/2009JB006482

Archean cratons might even lose their root completely, such as the North China craton [*Zheng et al.*, 2007].

[4] Diamonds derived from the lithospheric mantle and their occurrence place strong constraints on the thermal state of the lithosphere, because the stability field of diamond is restricted to relatively low temperatures along a continental geotherm (35–45 mW/m^2) at reasonable pressures (950–1350°C at 4.5–7.5 GPa [*Kennedy and Kennedy*, 1976; *Navon*, 1999]). That Archean cratonic lithosphere is relatively cold today was confirmed by heat flow measurements [*Jaupart and Mareschal*, 1999; *Pollack and Chapman*, 1977] and is consistent with seismic tomography models which show that positive shear wave velocity anomalies extend down to depths exceeding 200 km under cratonic crust [*Anderson and Bass*, 1984; *Polet and Anderson*, 1995; *Ritsema and van Heijst*, 2000; *Ritsema et al.*, 2004], indicating that the subcratonic mantle is significantly colder than younger subcontinental and suboceanic mantle.

[5] Geothermobarometry on mantle xenoliths and inclusions in diamonds also gives cold geotherms [*Boyd and Nixon*, 1975; *Boyd et al.*, 1985; *Finnerty and Boyd*, 1987; *MacGregor*, 1975; *O'Reilly and Griffin*, 2006; *Rudnick and Nyblade*, 1999]. However, these methods can only give snapshots of the temperature profile at certain times since xenolith derived geotherms reflect the state of the lithosphere at the time the xenolith was trapped in the kimberlite [*Boyd et al.*, 1985] (see also the 4-D lithospheric mapping approach of *O'Reilly and Griffin* [1996]). The evidence from the diamonds is therefore crucial since the preservation of diamonds that formed in the Archean unequivocally implies that the lithosphere must have been cold soon after its formation.

[6] Obtaining crystallization ages of diamonds, however, is notoriously difficult since diamonds do not contain any useful radioisotopes in sufficient quantities (see review by *Carlson et al.* [1999] for isotopic dating of diamonds). The aggregation of nitrogen defects in diamond is time dependent and can be used as a chronometer, particularly for relatively young diamonds (<100 Ma), but unfortunately, it is also strongly dependent on temperature [*Navon*, 1999]. Since the temperature evolution is usually not well constraint, the potential errors of the method are large. Therefore, diamond crystallization ages are commonly inferred from radiometric dating of their silicate or sulfide inclusions [*Carlson et al.*, 1999; *Navon*, 1999]. However, the dating of diamonds using their inclusions has been questioned. These doubts are based on a number of observations.

[7] 1. It is very difficult to conclusively show that an inclusion grew simultaneously with its host diamond due to the strong cubic diamond lattice that forces most inclusions to follow the diamond shape [*Bulanova*, 1995].

[8] 2. Inclusions in diamonds are small. For silicate inclusions, a large number of silicates from many different diamonds needs to be extracted to get enough material for isotope analysis, and the obtained age represents an average at best [*Navon*, 1999]. Today it is possible to date single sulfides by the Re-Os isotope technique, but it has been shown that this method produces erroneous results if the sulfide is not quantitatively extracted from the host diamond [*Richardson et al.*, 1993]. Moreover, the behavior of sulfides and sulfide melts in the mantle and during encapsulation in the diamond is not well understood [*Navon*, 1999].

[9] 3. Radiometric ages from inclusions in diamonds are usually model ages. This means they rely on assumptions about the isotopic evolution of the reservoir the inclusion grew from, which might not always be correct [*Rudnick et al.*, 1993].

[10] 4. It has been shown that different types of inclusions (silicates versus sulfides) or different techniques on one type of inclusion from a single diamond (e.g., U-Pb versus Re-Os on sulfides [*Carlson et al.*, 1999; *Rudnick et al.*, 1993]) can give very different age constraints [*Carlson et al.*, 1999; *Navon*, 1999]. Moreover, *Spetsius et al.* [2002] found sulfide inclusions with Archean Re-Os isotope ages in much younger (350 to 600 Ma) zircons, demonstrating that old sulfides can be inherited by younger hosts or that the Re-Os systematics of mantle sulfides might not be affected by their encapsulation in the diamond [*Navon*, 1999]. Hence, not all inclusions in diamonds are cogenetic, and it has been shown that diamonds do not exclusively form in the Archean [*Carlson et al.*, 1999; *O'Neill and Moresi*, 2003; *Richardson et al.*, 1990, 1993, 2004].

[11] Nevertheless, various authors have shown that the technical difficulties can be overcome by careful analyses of inclusions and their host diamond [*Carlson et al.*, 1999] and they have convincingly argued that some diamonds are indeed Archean [*Carlson et al.*, 1999; *Richardson and Harris*, 1997; *Richardson et al.*, 2001, 2004; *Westerlund et al.*, 2006]. Hence, even though it is difficult to constrain the exact thermal evolution of cratonic keels since the Archean, and we cannot exclude that cratonic keels experienced transient heating events, the occurrence of diamonds in kimberlites with eruption ages spanning from almost 2 Gyr (Premier, South Africa) to 45 Myr (Lac de Gras, Canada) implies that the conditions for diamond formation were definitely met at those times. It is also difficult to explain how large portions of mostly undeformed lithospheric mantle with Archean Re-Os ages could survive if the keels were significantly heated over extended periods of time. We therefore favor the most conservative model that explains the observations, that is that the Archean cratons preserved until today, including their more than 200 km thick lithospheric keels, formed at >2.5 Ga and have remained cold and stable ever since.

1.2. Previous Numerical Studies on Craton Stability

[12] Do numerical models support this conclusion based on petrology and geochemistry? More precisely, what is the result of systematic dynamic modeling of synthetic scenarios of long-term stability of the lithosphere? Not surprisingly, given the poorly constrained rheological parameters and the enormous extrapolation in both time and space, modeling results do not provide a conclusive answer (see review by *King* [2005]). Whereas some authors [*Lenardic et al.*, 2003; *O'Neill et al.*, 2008; *Shapiro et al.*, 1999; *Sleep*, 2003] find long-term survival of the cratonic root based on their modeling, several others observe lithosphere instability in their models [*Cooper et al.*, 2004; *Doin et al.*, 1997; *Lenardic and Moresi*, 1999; *Lenardic et al.*, 2000; *O'Neill and Moresi*, 2003].

[13] Recently, however, the inability of some models to reproduce long-term craton stability has been used as an argument to question the significance of the old ages obtained from inclusions in diamonds [*O'Neill and Moresi*,

2003] (see also review by *King* [2005]). These models suggest that chemical buoyancy and the strength of cold and depleted lithosphere are not sufficient to resist deformation and gradual thermal erosion of cratonic keels by mantle convection and plate subduction. [*O'Neill and Moresi*, 2003] have, for example, investigated craton stability in a plate tectonics-like regime with active surface tectonics. They found that whereas the chemical component of cratonic lithosphere can be preserved through time, the conditions for diamond stability in the cratonic keel were not continuously met over long geological times (>1 Ga). The reason for this was the convective removal of the basal thermal boundary layer of the cratonic keel in their models which allowed temperature fluctuations to occur inside the keel. Yet, in that study and other previous models, temperature-dependent viscosity ratios between cold lithosphere and hot convecting mantle were fixed at a constant, relatively low value of 10^5 [*Cooper et al.*, 2004, 2006; *de Smet et al.*, 2000; *Doin et al.*, 1997; *Lenardic and Moresi*, 1999; *Lenardic et al.*, 2000, 2003; *O'Neill and Moresi*, 2003; *O'Neill et al.*, 2008; *Shapiro et al.*, 1999; *Sleep*, 2003], whereas in laboratory creep experiments, viscosity ratios between cold cratonic lithosphere and convecting mantle were found to be orders of magnitude larger than this (see section 1.3). While the extrapolation of laboratory values to geologic strain rates is notoriously difficult, it appears possible that the apparent instability of cratonic lithosphere in some previous models may have resulted from the assumed low temperature-dependent viscosity ratio.

[14] *Lenardic and Moresi* [1999] point out that larger temperature-dependent viscosity ratios could well account for long-term craton stability but would do so by the sacrifice of plate tectonics; for large temperature-dependent viscosity ratios, a stagnant lid forms in the uppermost part of the model, thereby prohibiting any active surface tectonics. Therefore, in a later study [*Lenardic et al.*, 2003], they incorporate plastic yielding and postyield weakening into their model in order to enable plate tectonics-like behavior with subduction of plates. They found that whereas low friction coefficients <0.15 are required for the oceanic lithosphere in order to sustain active surface tectonics (which agrees with a previous study by *Moresi and Solomatov* [1998]), friction coefficients in the cratonic crust and mantle lithosphere need to be at least 4 times higher in order to account for long-term preservation of cratonic roots. If in their models a bulk friction coefficient >0.15 is chosen instead, they observe a transition to stagnant lid convection.

[15] While the aforementioned studies convincingly showed that plate subduction has the potential to effectively erode and destabilize cratonic lithosphere, it remains unclear how frequent and common this processes is. The geologic record shows, in fact, that continents tend to rift and rupture along preexisting weak zones. As a consequence, cratons are often surrounded by younger, relatively weak mobile belts which may effectively buffer them from subduction erosion [*Lenardic et al.*, 2000, 2003, and references therein].

[16] In this paper, we therefore return to the problem on how cratons can avoid erosion by ambient mantle flow. Using improved numerical techniques for stagnant lid convection, we explore how realistic temperature-dependent viscosities and viscoelastic effects control craton stability. The models presented here are based on conservative extrapolation of laboratory creep experiments [*Karato and Wu*, 1993] and take into account that the cold upper portion of the continental lithosphere behaves elastically, which is supported by a large number of observations [*Burov et al.*, 1998; *Burov and Diament*, 1995; *Watts*, 1992; *Watts and Zhong*, 2000], by application of a viscoelastic rheology. These advances in numerical techniques allow us to critically review the stability of cratonic lithosphere in the stagnant lid regime and, due to the better viscoelastic stress estimates, will serve as a basis for improved future models that include plate tectonics.

1.3. Viscosity Ratios Between the Lithosphere and the Convecting Mantle

[17] Viscosity estimates of the Earth mantle can either be derived from natural observations or from laboratory creep experiments conducted on mantle rocks. For the asthenosphere, viscosity estimates have mainly been derived from studies of three different geological processes: (1) postglacial rebound, i.e., estimation of the uplift rate after removal of ice load, (2) flexure of the lithosphere at subduction trenches and under loading by seamounts and volcanic islands, and (3) migration of the foreland bulge in alpine foreland basins. The rheological model underlying those estimates is that of a viscous substratum (asthenosphere) overlain by an elastic plate of finite thickness. Through these methods, reliable viscosity estimates have been obtained for the asthenosphere and the underlying mantle (see *Burov and Diament* [1995], *Watts* [1992], and *Watts and Zhong* [2000] for reviews and contributions). For cratonic lithosphere however, viscosity estimates are more difficult to obtain from natural observations, since it hardly deforms through time, but instead behaves as a rigid, elastic plate [*Watts and Zhong*, 2000], the viscosity of which can be considered infinite [*Lowrie*, 2007, p. 114]. *Burov et al.* [1998], e.g., determine the effective elastic thickness (EET) of the Canadian cratonic shield area to be around 100–120 km. Determination of viscosity for undeformed, stable cratonic lithosphere is notoriously difficult, since measurements of viscosity require deformation. Given the poor constraints for viscosities in undeformed lithosphere, one can turn to laboratory experiments to get an idea about the expected order of magnitude. The experimentally determined creep law for polycrystalline mineral assemblages [*Karato and Wu*, 1993] indicates a strong exponential dependence of viscosity of mantle minerals on temperature:

$$\dot{\varepsilon} = A\left(\frac{\sigma}{G}\right)^n \left(\frac{b}{d}\right)^m \exp\left(-\frac{E_a + pV_a}{RT}\right). \quad (1)$$

[18] Here, $\dot{\varepsilon}$, σ, A, G, b, d, n, m, E_a, p, V_a, R and T are shear strain rate (scalar), shear stress (scalar), preexponential factor, elastic shear modulus, length of the Burgers vector, grain size, stress exponent, grain size exponent, activation energy, pressure, activation volume, gas constant and temperature, respectively. All parameters used in this paper are also compiled in the notation section for convenience.

[19] Since olivine is commonly assumed to dominate mantle peridotite rheology, we can use the creep law (1) and experimentally obtained parameter values for polycrystalline, dry olivine aggregates from *Karato and Wu* [1993] and calculate approximate, hypothetical viscosities for the upper

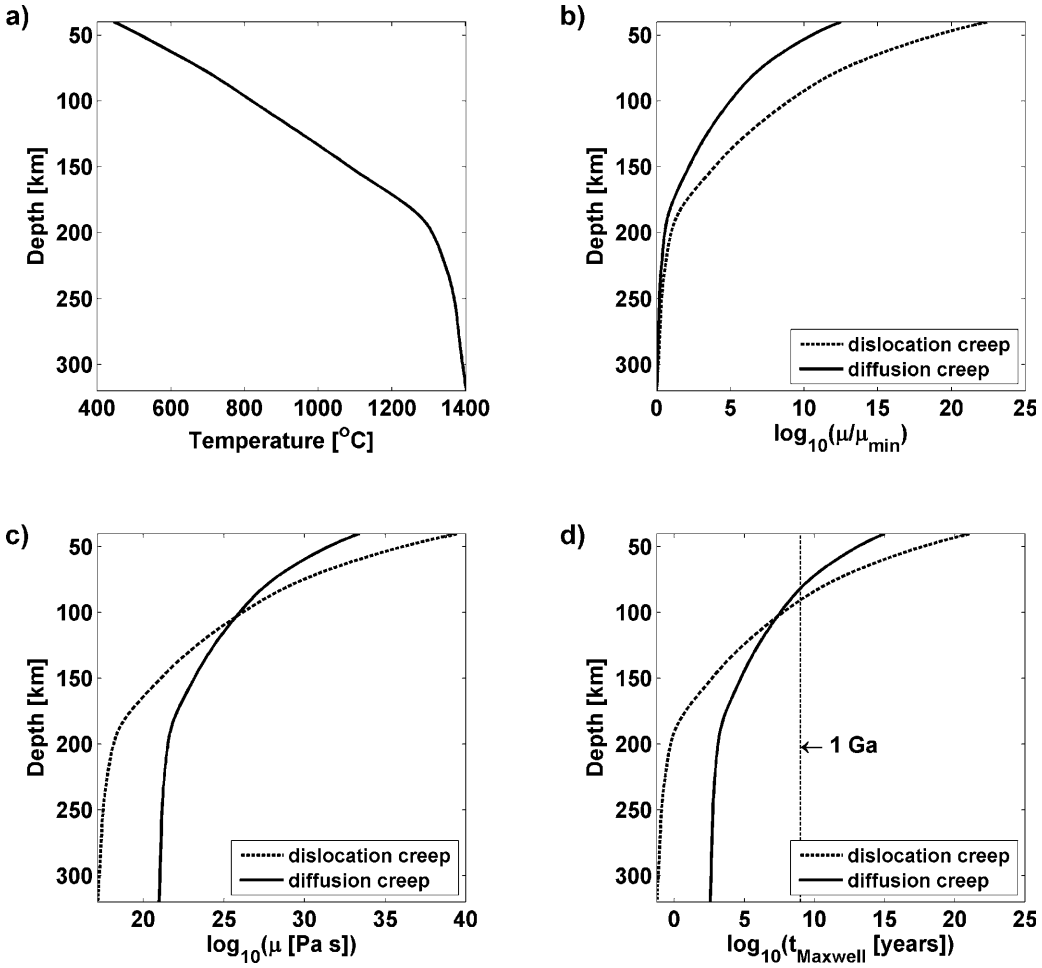

Figure 1. (a) Temperature profile through cratonic lithosphere as derived from geothermobarometry on xenoliths from the Kalahari craton after *Rudnick and Nyblade* [1999] with conductive geotherm in the lithospheric upper half and an adiabatic geotherm in the convecting lower half of the profile. We restrict the evaluation of viscosities to depths below 40 km, since the creep law employed is only valid for mantle rocks; that is, the crustal section is neglected here. (b) Temperature-dependent viscosity ratios for diffusion and dislocation creep (normalized to respective minimal viscosity values $\mu_{\min}$) calculated from mineral creep law and experimentally derived parameters for dry olivine aggregates from *Karato and Wu* [1993]. (c) Same as Figure 1b but with dimensional viscosity values (no normalization). (d) Maxwell relaxation time $t_{Maxwell}$ for the viscosity profiles given in Figure 1c. Note logarithmic scales in Figures 1b–1d.

continental mantle for a given cratonic geotherm. The results for an exemplary geotherm from the Kalahari craton [*Rudnick and Nyblade*, 1999] are given in Figure 1.

[20] Figure 1d also shows the strong increase of Maxwell relaxation time with viscosity for a fixed value of elastic shear modulus G. The degree of elastic response of viscoelastic materials can be described by the characteristic Maxwell relaxation time $t_{Maxwell}$ which expresses how long it takes for stress in the viscoelastic material to relax to 1/e of its original value after an initial deformation:

$$t_{Maxwell} = \frac{\mu(T)}{G}. \tag{2}$$

[21] The exponential temperature dependence of viscosity in (1) produces a viscosity ratio $\mu_r = \mu(T_{\min}))/\mu(T_{\max})$ of many orders of magnitude between the cold lithospheric lid and the sublithospheric mantle (Figure 1b). Such high viscosities (see also Figure 1c) indicate that the upper part of the lithospheric mantle does effectively not creep on geological time scales, but instead behaves as a rigid, elastic lid. For Archean cratonic lithosphere which represents the coldest and strongest part of all continental lithosphere, this must clearly be the case. The fact that lithosphere exhibits elastic response even on long time scales can readily be seen from the associated long Maxwell relaxation times in Figure 1d (see section 4.3 for details).

2. Methods

2.1. Governing Equations

[22] We solve the conservation equations of mass, momentum and energy for a viscoelastic, incompressible (Boussinesq approximation) fluid at infinite Prandtl number, i.e., for inertialess flow.

[23] From conservation of mass for incompressible fluids, we obtain the equation of continuity

$$\frac{\partial v_i}{\partial x_i} = 0, \tag{3}$$

where v_i and x_i are velocity and Eulerian coordinates vectors, respectively. For infinite Prandtl number convection, conservation of momentum simplifies to the stress equilibrium equation

$$\frac{\partial \tau_{ij}}{\partial x_j} - \frac{\partial p}{\partial x_i} - \rho_0 g \alpha (T - T_0)\hat{\mathbf{z}} = 0, \tag{4}$$

where τ_{ij}, p, ρ_0, g, α and $\hat{\mathbf{z}}$ are the deviatoric stress tensor, pressure, density at reference temperature T_0 (temperature at the hot bottom), acceleration due to gravity, thermal expansion coefficient and a unit vector pointing vertically downward, respectively. For a Maxwell viscoelastic rheology, the constitutive equation is

$$\dot{\varepsilon}'_{ij} = \frac{1}{2\mu(T)}\tau_{ij} + \frac{1}{2G}\frac{\mathcal{D}\tau_{ij}}{\mathcal{D}t} \tag{5}$$

with

$$\frac{\mathcal{D}\tau_{ij}}{\mathcal{D}t} = \frac{\partial \tau_{ij}}{\partial t} + v_k \frac{\partial \tau_{ij}}{\partial x_k} - \omega_{ik}\tau_{kj} - \omega_{jk}\tau_{ik} \tag{6}$$

being the Jaumann invariant stress derivative which we chose to apply in our model. Here, $\dot{\varepsilon}'_{ij}$ and ω_{ij} denote the deviatoric strain rate and vorticity tensors, respectively, and μ, G and t are shear viscosity, elastic shear modulus and time. Viscosity μ is exponentially dependent on temperature T as described by equation (10). Due to the incompressibility condition (3), deformation can be fully described in terms of deviators. The deviatoric stress tensor τ_{ij} is related to the total stress tensor σ_{ij} through $\tau_{ij} = \sigma_{ij} - 1/3\sigma_{kk}\,\delta_{ij} = \sigma_{ij} + p\delta_{ij}$ and, analogously, deviatoric strain rate $\dot{\varepsilon}'_{ij}$ is related to bulk strain rate $\dot{\varepsilon}_{ij}$ through $\dot{\varepsilon}'_{ij} = \dot{\varepsilon}_{ij} - 1/3\dot{\varepsilon}_{kk}\,\delta_{ij}$, where δ_{ij} is the Kronecker delta. The strain rate tensor is defined as

$$\dot{\varepsilon}_{ij} = \frac{1}{2}\left(\frac{\partial v_i}{\partial x_j} + \frac{\partial v_j}{\partial x_i}\right) \tag{7}$$

and the vorticity tensor as

$$\omega_{ij} = \frac{1}{2}\left(\frac{\partial v_j}{\partial x_i} - \frac{\partial v_i}{\partial x_j}\right). \tag{8}$$

[24] Conservation of energy for incompressible fluids simplifies to the advection-diffusion equation for temperature T

$$\frac{\partial T}{\partial t} = \frac{\partial}{\partial x_i}\left(\kappa \frac{\partial T}{\partial x_i}\right) - v_i \frac{\partial T}{\partial x_i}, \tag{9}$$

where κ is the heat diffusivity. We use the Frank-Kamenetskii approximation

$$\mu(T) = \mu_0 \exp(-\gamma(T - T_0)) \tag{10}$$

to account for the temperature-dependent viscosity variations in the creep law (1). In (10), μ_0 is the reference viscosity at the hot bottom and γ is a creep activation $\gamma = E_a/(RT_0^2)$. As *Solomatov and Moresi* [1996, 2000] point out, the representation of the temperature dependence of viscosity using the Frank-Kamenetskii law gives identical results to the Arrhenius-type temperature dependence in the creep law (1) for the limit of large viscosity ratios, as is the case in our simulations. We neglect pressure dependence of viscosity. *O'Neill et al.* [2008] explored the effect of pressure dependence of viscosity on craton stability and showed that convection becomes more sluggish with increasing pressure dependence, resulting in prevention of stress excursions inside the craton. Thus, pressure-dependent viscosity enhances craton stability. We also neglect internal heat generation by radioactive decay of heat producing elements. As *Garfunkel* [2007] pointed out, heat production in the Archean lithosphere is, due to extensive melt extraction during its differentiation, even smaller than in the primitive mantle, resulting in negligible influence on the geotherm. *Jaupart and Mareschal* [1999] and *Michaut and Jaupart* [2007] agree that heat production must be negligible within cratonic lithosphere, since it would otherwise become mechanically unstable due to creep activation and not exhibit long-term stability. Craton stability under conditions of the Archean with heat production of the ambient mantle 3–4 times higher the present value was studied by *O'Neill et al.* [2008]. Their study concludes that higher mantle heat production renders cratons more stable than at present-day conditions since stresses exerted on the cratons are lower due to the lower viscosities in a hotter mantle. Thus, by neglecting both pressure dependence of viscosity and internal heat production, we model a worst-case scenario for stability of our model craton.

2.2. Nondimensionalization

[25] The independent parameters domain height $\tilde{h}$, viscosity at the hot bottom $\tilde{\mu}_0$, heat diffusivity $\tilde{\kappa}$ and the temperature difference throughout the domain $\Delta\tilde{T}$ are used as scales to nondimensionalize the governing equations. Substitution of the scaled parameters into the governing equations results in three nondimensional parameters: the Rayleigh number for bottom heating convection Ra, the Deborah number De and a creep activation parameter λ. The Deborah number De measures the ability of a material to "flow," i.e., to deform by viscous creep. The term "Deborah number" was first coined by *Reiner* [1964] and was inspired by the statement "The mountains flowed before the Lord" of Deborah in the Bible (Judges 5:5). For the limiting cases $De = 0$, the material behaves as a Newtonian liquid; for $De = \infty$ it behaves as an elastic solid. We define the Deborah number as the ratio of a reference Maxwell viscoelastic relaxation time $t_{Maxwell,ref} = \tilde{\mu}_0/G$ at viscosity μ_0 to a thermal diffusion time $t_{Diffusion} = \tilde{h}^2/\tilde{\kappa}$.

$$Ra = \frac{\rho_0 g \alpha \Delta\tilde{T}\tilde{h}^3}{\tilde{\kappa}\tilde{\mu}_0}, \tag{11}$$

$$De = \frac{\tilde{\mu}_0\tilde{\kappa}}{G\tilde{h}^2} = \frac{t_{Maxwell,ref}}{t_{Diffusion}}, \tag{12}$$

$$\lambda = \frac{E_a \Delta\tilde{T}}{RT_0^2}. \tag{13}$$

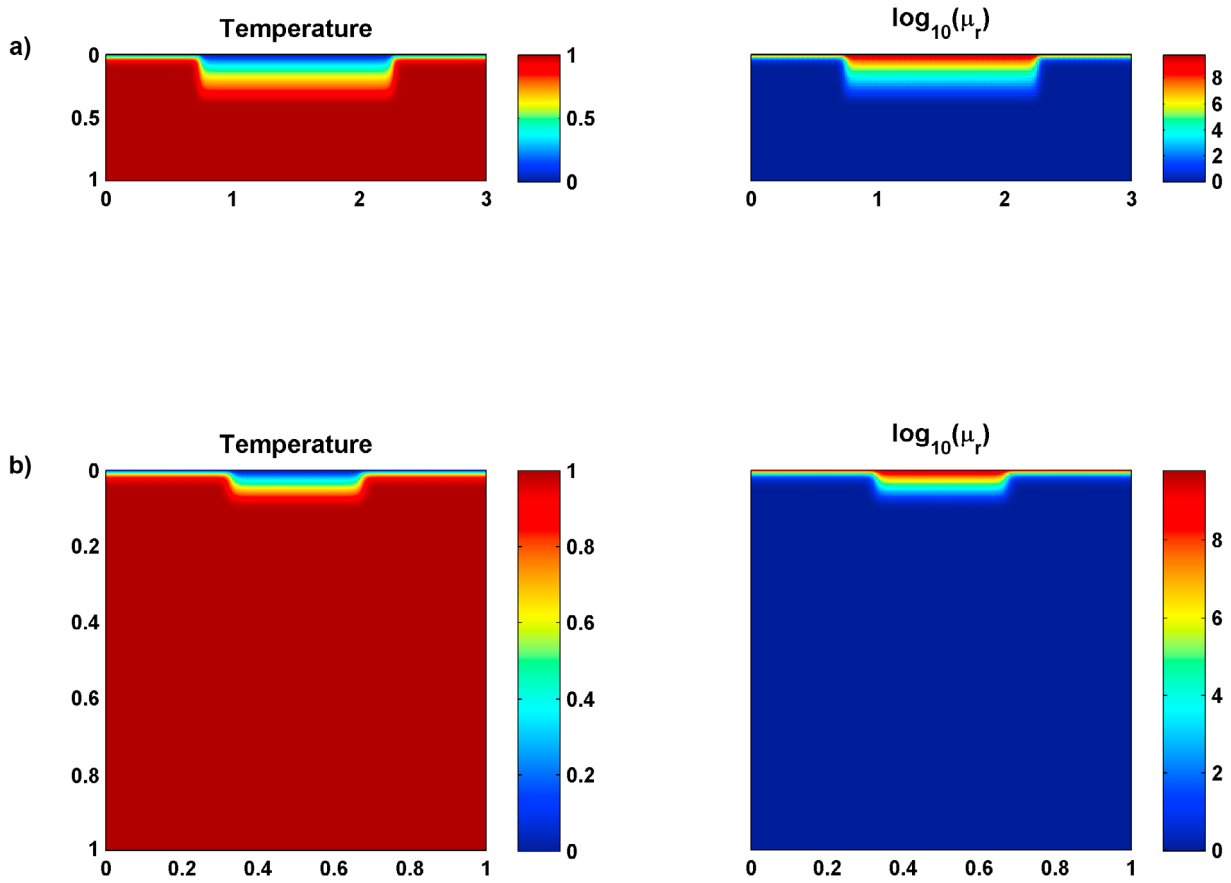

Figure 2. Model setup and initial temperature condition for (a) upper mantle and (b) whole mantle simulations. (left) Initial temperature distribution. (right) Initial temperature-dependent viscosity distribution (logarithmic scale). The craton is defined by an initial cold temperature anomaly with low geothermal gradient down to 250 km depth. The remaining part of the model is initialized with constant maximum temperature. Grid resolution is (a) 450 × 100 and (b) 450 × 300.

The resulting nondimensional form (asterisk denotes nondimensional parameters and variables) of the governing equations is

$$\frac{\partial v_i^*}{\partial x_i^*} = 0, \tag{14}$$

$$\frac{\partial \tau_{ij}^*}{\partial x_j^*} - \frac{\partial p^*}{\partial x_i^*} - Ra(T - T_0)^* \hat{\mathbf{z}} = 0, \tag{15}$$

$$2\mu^*\left(T^*\right)\dot{\varepsilon}_{ij}^{\prime *} = \tau_{ij}^* + De\mu^*\left(T^*\right)\frac{\mathrm{D}\tau_{ij}^*}{\mathrm{D}t^*}, \tag{16}$$

$$\frac{\partial T^*}{\partial t^*} = \frac{\partial^2 T^*}{\partial x_i^{*2}} - v_i^* \frac{\partial T^*}{\partial x_i^*}, \tag{17}$$

$$\mu^*\left(T^*\right) = \exp\left(-\lambda(T - T_0)^*\right). \tag{18}$$

The nondimensional creep activation parameter λ is chosen such that it produces a specific maximum viscosity ratio $\mu_r(T) = \mu(T_{\min})/\mu(T_{\max}) = \exp(\lambda^*)$ throughout the domain.

2.3. Numerical Methods

[26] The theoretical background of our finite element method (FEM) code VEMAN which we used for the presented simulations and technical details concerning the implementation of a Maxwell viscoelastic rheology are described by *Beuchert and Podladchikov* [2010].

2.4. Model Setup

[27] The governing equations are integrated on a regular two-dimensional, rectangular finite element grid. The initial temperature is set to maximum (lower boundary) temperature to provide the worst-case scenario initial conditions. As additional initial temperature condition, a model craton, represented by a rectangular, steady state conduction temperature profile, is inserted in the top center of the domain (Figure 2). The ratio of craton height (250 km) to the domain height is chosen such that the domain represents either (1) the upper mantle (660 km) or (2) the whole mantle (2890 km). Top and bottom boundaries are isothermal with minimum and maximum temperature, respectively, and allow for free-slip (zero traction boundaries). In order to obtain a fixed reference frame in horizontal direction, we prescribe $v_x = 0$ at one grid point at the top center. The sides of the domain are periodic (wrap-around) in order to mini-

mize boundary effects. The grid resolution is 450 × 100 (horizontal × vertical) for the upper mantle simulations and 450 × 300 for the whole mantle simulations. The grid is refined at the top and bottom boundaries in order to capture small-scale dynamics within the thermal boundary layers.

[28] Upper mantle simulations were done in order to be able to compare the results with previous modeling from other authors whose models comprised the upper mantle only [*Cooper et al.*, 2004; *Doin et al.*, 1997; *Lenardic and Moresi*, 1999; *Lenardic et al.*, 2000, 2003; *O'Neill and Moresi*, 2003; *Shapiro et al.*, 1999; *Sleep*, 2003]. Additionally, we chose to set up a model for the whole mantle depth, as recently also done by *O'Neill et al.* [2008], in order to avoid the introduction of an artificial lower boundary at 660 km. If models comprise only the upper mantle, zero flux across the 660 km discontinuity is assumed; yet, this boundary condition would only be realistic if mantle convection was layered. Yet, it is evident from observation of penetration of slabs [*Grand*, 2002; *Gu et al.*, 2001; *van der Hilst*, 1995; *van der Hilst et al.*, 1997] and plumes [*Montelli et al.*, 2004; *Ritsema and Allen*, 2003] through the 660 km discontinuity in seismic velocity models that while the 660 km discontinuity impedes mantle flow to a certain degree, convection still comprises the whole mantle. Consequently, introduction of an impermeable boundary at the base of the upper mantle in numerical models is unrealistic. In whole mantle models instead, the core-mantle boundary (CMB) represents a natural lower boundary through which convection does not penetrate [*Gurnis et al.*, 1998]. This interpretation is based on the sharpness and the strong chemical differences between silicate mantle and iron core [*Morelli and Dziewonski*, 1987].

[29] Compositional buoyancy of cratons, whereas being a prerequisite for gravitational stability of cratons [*Jordan*, 1978], has been found to play only a minor role for craton stabilization in previous studies, i.e., compositional buoyancy alone cannot provide for long-term stability of cratonic roots [*Doin et al.*, 1997; *Lenardic and Moresi*, 1999; *Lenardic et al.*, 2003; *Shapiro et al.*, 1999; *Sleep*, 2003]. We therefore chose to exclude compositional buoyancy from our modeling investigation and to only study the more important erosive effects of mantle convection on cratonic root preservation. Yet, we imposed neutral buoyancy of the craton by fixing the model craton to the top boundary in vertical direction (v_y(top) = 0), but allow for free slip. Since negative buoyancy of the cratonic root can still contribute to root instability in our model, we model a worst-case scenario in terms of gravitational root stability.

[30] We also chose not to include the effects of chemically enhanced viscosity of the cratonic lithosphere in our model and thus also simulate a worst-case scenario in terms of erosive stability of the craton.

3. Results

3.1. Upper Mantle Simulation

[31] We first present the temporal evolution for an upper mantle model with low (Figure 3) and high (Figure 4) temperature-dependent viscosity ratios. When we apply a relatively low viscosity ratio of $\mu_r = 10^5$, a value used, e.g., by *Lenardic et al.* [2003] and *O'Neill and Moresi* [2003], the model craton is thermally eroded in our simulations on the order of 100 Myr (Figure 3). For low viscosity ratios, craton destruction results mostly from the effect of edge-driven convection at the sides of the craton, triggered by the horizontal temperature gradient between cold cratonic lithosphere and hot convecting mantle, an effect discussed in detail, e.g., by *King and Ritsema* [2000], but also by ascending plumes and basal viscous drag, the latter of which was explored by *Garfunkel* [2007]. When instead a high viscosity ratio $\mu_r = 10^{10}$ is applied, the model craton remains thermally stable in our stagnant lid model during the entire simulation time of 500 Myr (Figure 4, see also Animation S1 in the auxiliary material for an animation of the temporal temperature evolution of upper mantle simulations with low and high viscosity ratios).[1]

[32] For quantitative analysis, the results of which are presented in Figures 6, 10 and 11, we defined a thermal stability criterion for survival of the model craton. Our stability criterion is that the base of the thermal lithosphere, as defined by the 1200°C isotherm (or $T/\Delta T$ = 1200°C/1400°C ≈ 0.86 in nondimensional form), remains within the diamond stability field, i.e., below the graphite-diamond transition (GDT), throughout a specific long geological time (1 Gyr). Since only temperatures higher than the initial temperature would result in instability of the craton, we compute the mean geotherm from the maximum temperature recorded at any point below the craton during the simulation. For the high viscosity ratio simulation ($\mu_r = 10^{10}$, blue curves in Figure 5), this geotherm remains low and close to the initial geotherm (solid circle in Figure 5) throughout the simulation, whereas it continually rises in the low viscosity ratio simulation ($\mu_r = 10^5$, red curves in Figure 5). When the geotherm rises, old diamonds initially formed within the lithosphere are destroyed implying thermal instability of the cratonic keel. We define the time until the geotherm crosses the temperature at the base of the thermal lithosphere (crossed open circle in Figure 5, corresponding to $T/\Delta T$ = 0.86 as given above) on the graphite-diamond transition (black line in Figure 5 [after *Kennedy and Kennedy*, 1976]) as the time to instability $t_{unstable}$.

[33] Using the stability criterion mentioned above, we explored a range of Rayleigh numbers *Ra* and viscosity ratios μ_r to determine at which parameter combinations the model craton remains stable for a long geological time or instead becomes unstable; for the latter case, we determined the dependence of the time until instability on *Ra* and μ_r. The circles in Figure 6 show the parameter combinations of individual runs. Solid circles indicate runs where the model craton was stable for more than 1 Gyr, crossed open circles are plotted when instability occurred within less than 1 Gyr. Color contours show the time to instability $t_{unstable}$ (in years, logarithmic scale).

3.2. Whole Mantle Simulation

[34] For the whole mantle simulations, the bottom heating Rayleigh number is, due to scaling of the Rayleigh number with domain height, almost two orders of magnitude higher than for the upper mantle simulations. As can be seen in Figure 7 for a simulation with Rayleigh number $Ra = 10^9$, convection becomes significantly more turbulent than in the

[1] Auxiliary materials are available in the HTML. doi:10.1029/2009JB006482.

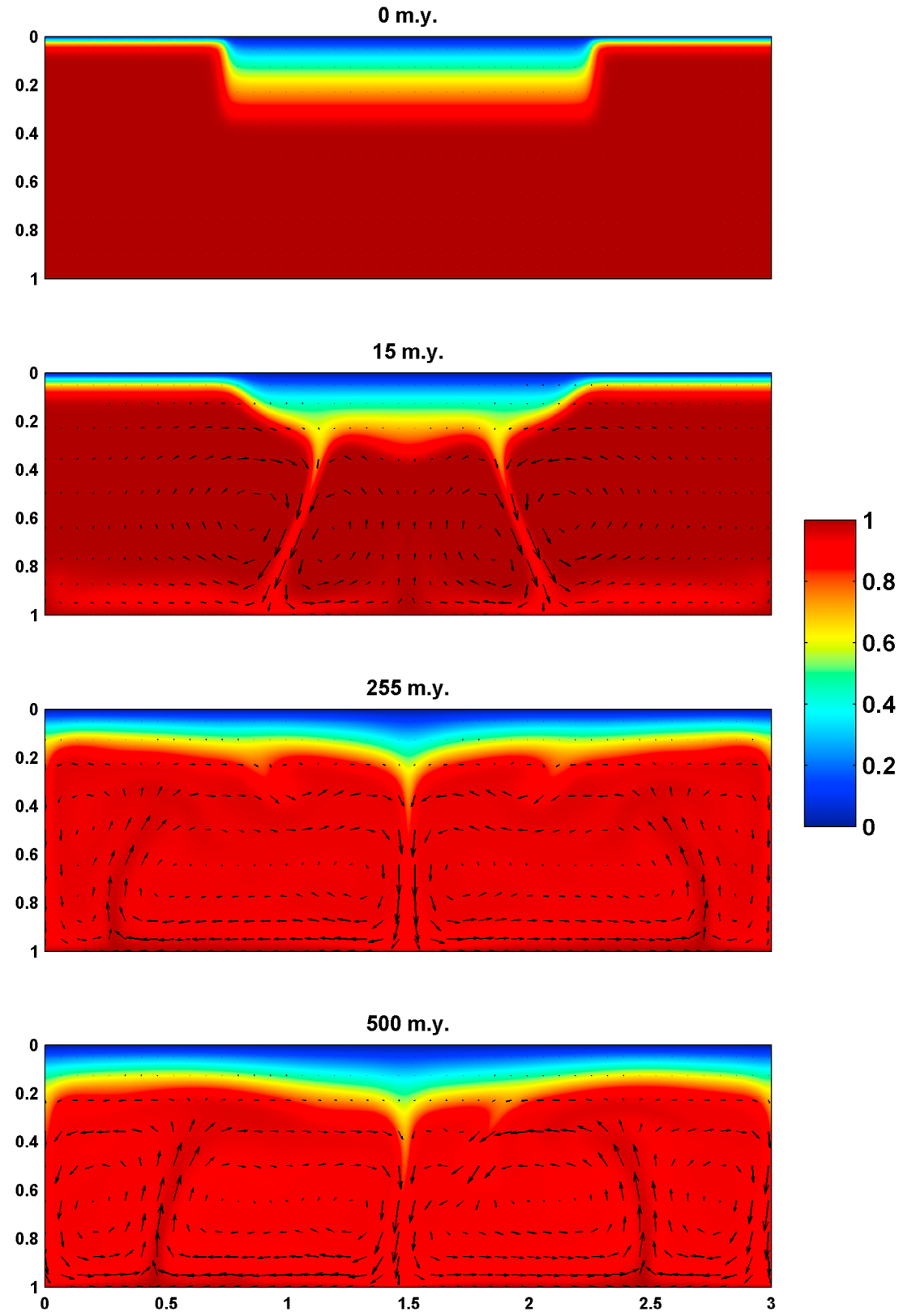

Figure 3. Temporal evolution of the temperature field in a mantle convection simulation with Rayleigh number $Ra = 2 \times 10^7$ and viscosity ratio $\mu_r = 10^5$. The cratonic keel (defined by a cold temperature anomaly, see setup in Figure 2a) is readily eroded away on the order of 100 Myr by the vigor of convection currents in this relatively low viscosity ratio regime. The base of the thermal lithosphere exits the diamond stability field for this low viscosity ratio simulation (red in Figure 5), indicating that for such viscosity ratio the cratonic keel is not stable.

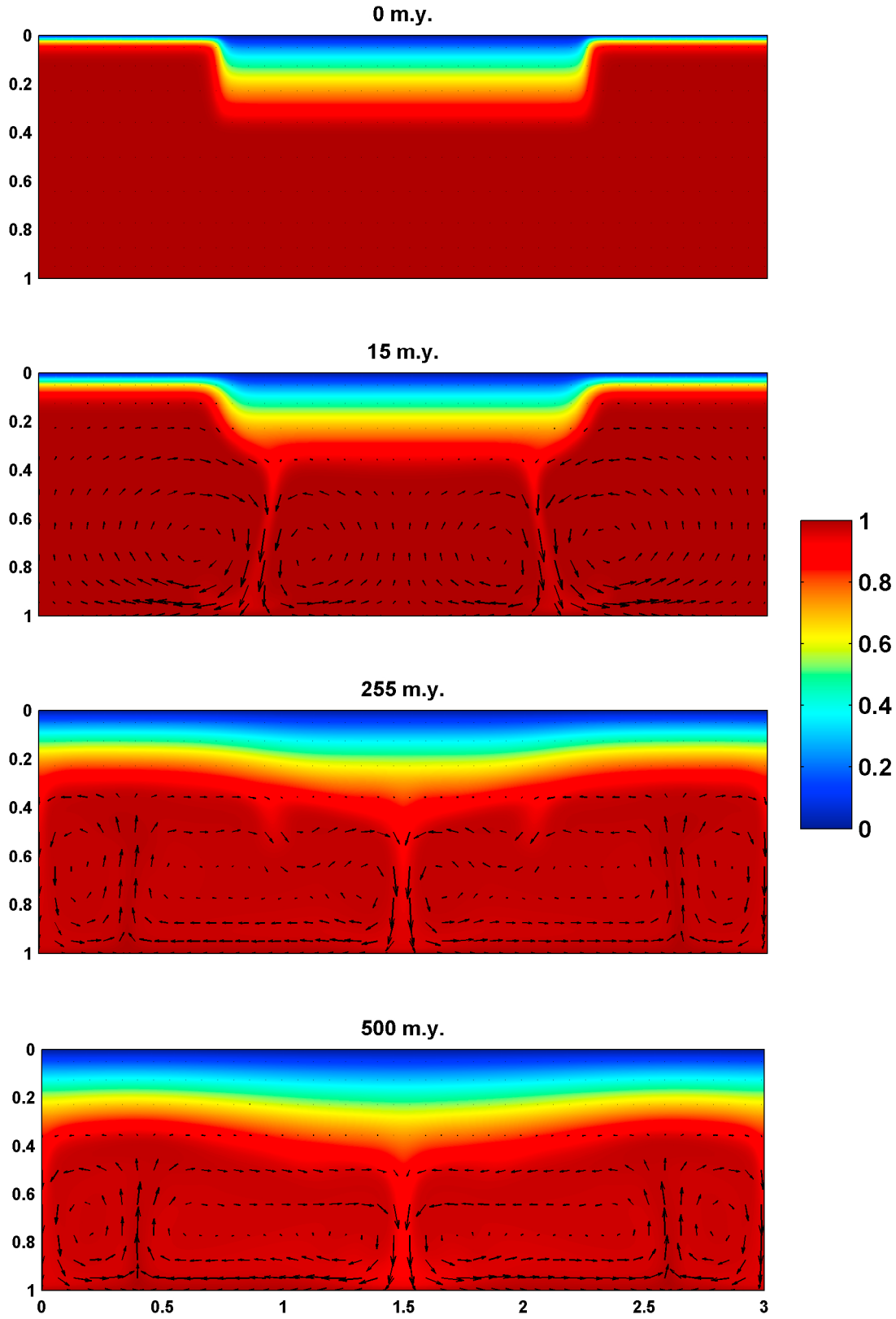

Figure 4. Temporal evolution of the temperature field in a mantle convection simulation with Rayleigh number $Ra = 2 \times 10^7$ and viscosity ratio $\mu_r = 10^{10}$. The cratonic keel remains stable throughout the entire simulation of 500 Myr due to the high temperature-dependent viscosity ratio. The base of the thermal lithosphere remains within the diamond stability field for this high viscosity ratio simulation (blue in Figure 5) throughout the entire simulation, indicating long-term stability of the cratonic keel.

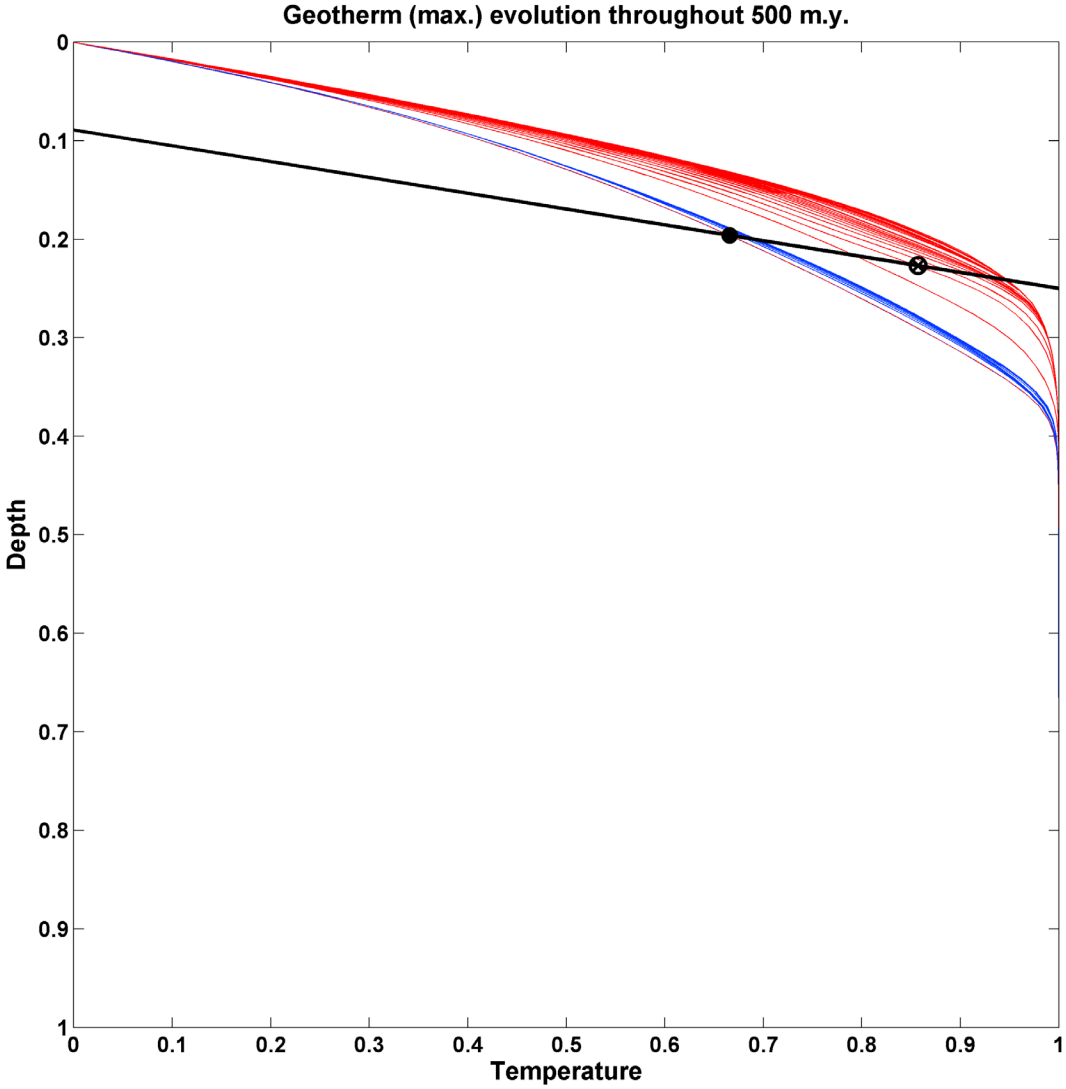

Figure 5. Mean geotherm below the craton for the highest temperatures recorded at intervals of 10 Myr for runs with low (red, $\mu_r = 10^5$) and high (blue, $\mu_r = 10^{10}$) viscosity ratios at a bottom heating Rayleigh number $Ra = 2 \times 10^7$. The total simulation time is 500 Myr. The black solid line shows the graphite-diamond transition (GDT) from *Kennedy and Kennedy* [1976]. The solid circle marks the intersection of the initial geotherm (equivalent for both runs) with the GDT, and the crossed open circle marks the intersection of the GDT with the nondimensional temperature at the base of the thermal lithosphere (see text for explanation). Our criterion for craton stability is that the base of the thermal lithosphere remains below the GDT throughout the entire simulation time. This is the case for the high viscosity ratio simulation (blue) but not for the low viscosity ratio run (red).

upper mantle simulations with $Ra = 2 \times 10^7$ (Figure 3). Whereas the model craton is eroded on the order of 100 Myr for a low viscosity ratio $\mu_r = 10^5$ (Figure 7), it remains stable for >1 Gyr in the high viscosity ratio simulation with $\mu_r = 10^{10}$ (Figure 8).

[35] As for the upper mantle simulation (Figure 5), the recorded maximal geotherm below the craton remains low for the high viscosity ratio simulation ($\mu_r = 10^{10}$, blue curves in Figure 9), but continually rises in the low viscosity ratio simulation ($\mu_r = 10^5$, red curves in Figure 9), indicating craton stability and erosion for the former and latter case, respectively. The stability criterion is equivalent to the one described in section 3.1 for the upper mantle simulations.

[36] As in section 3.1 for the upper mantle setting, we conducted a sequence of simulations in order to derive a quantitative relation between Rayleigh number Ra, viscosity ratio μ_r and time to instability $t_{unstable}$ of the model craton for the whole mantle setting. The explored parameter range is shown in Figure 10.

3.3. Data Analysis

[37] In Figure 11, we present the data collapse of our numerical results where instability occurred in the upper and

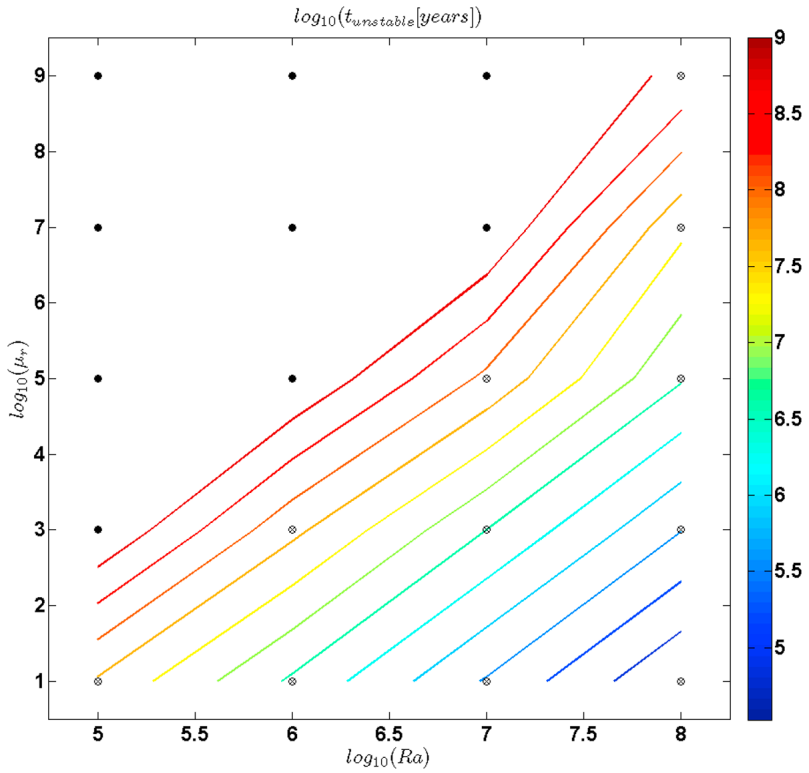

Figure 6. Explored range of Rayleigh numbers Ra and viscosity ratios μ_r for the upper mantle setting. Solid circles represent runs where the craton remained stable throughout the simulation time of 1 Gyr, and crossed open circles represent runs where the craton became unstable. For runs where instability occurred within 1 Gyr, the time to instability $t_{unstable}$ is contoured in colors (in years, logarithmic scale).

whole mantle simulations (contours in Figures 6 and 10, respectively). Since we were interested to see whether there is a significant difference in terms of craton stability between viscous and viscoelastic rheologies, we additionally conducted simulations for the same parameter range using a viscous rheology (Figure 11, open circles). The data fit indicates that there is no significant dependence of the time to craton instability $t_{unstable}$ on the applied rheology (linear viscous or viscoelastic).

[38] From our simulations for upper and whole mantle (see data fit in Figure 11), we derived the following dependence of the nondimensional time to instability $t_{unstable}^*$ on Ra, μ_r and the relative height of the initial perturbation δ_c:

$$t^*_{unstable} = 50\delta_c \frac{\sqrt{\mu_r}}{Ra}, \tag{19}$$

where δ_c is the ratio of the domain height h to the thickness of the initial perturbation, i.e., the model craton, z_c:

$$\delta_c = \frac{h}{z_c}. \tag{20}$$

[39] We conclude that the temperature-dependent viscosity ratio is critical for the question of cratonic root stability in stagnant lid models. Large viscosity ratios are here sufficient to prevent cratonic erosion for billions of years even for high Rayleigh numbers. Whether this is the case in models with plate tectonics remains to be explored.

[40] Figure 12 shows the dependence of $t_{unstable}$ on the initial thickness of the model craton z_c according to (19) for a viscosity ratio $\mu_r = 6.9 \times 10^7$ calculated for dry olivine after *Solomatov and Moresi* [1996] in the frame of the Frank-Kamenetskii approximation and for a range of Rayleigh numbers. The plot demonstrates (1) that the cratonic keel exhibits long-term stability for realistic viscosity ratio and realistically high Rayleigh numbers for the whole mantle and (2) that the uncertainty about the initial thickness of the craton is of minor concern for the question of its stability, since $t_{unstable}$ mainly depends on the Rayleigh number (for a given viscosity ratio).

4. Discussion

4.1. Stagnant Lid Versus Plate Tectonics Regime

[41] As several workers [e.g., *Lenardic and Moresi*, 1999; *Lenardic et al.*, 2003; *Moresi and Solomatov*, 1998] point out, the stagnant lid regime is not directly applicable to Earth, since our planet is in a plate tectonics regime with individual plates subducting, drifting apart or past each other. In order to approach a more realistic regime, some previous studies that addressed craton stability therefore included oceanic lithosphere spreading and subducting slabs [*Doin et al.*, 1997] or introduced a plastic yield criterion combined with postyield weakening that produces plate

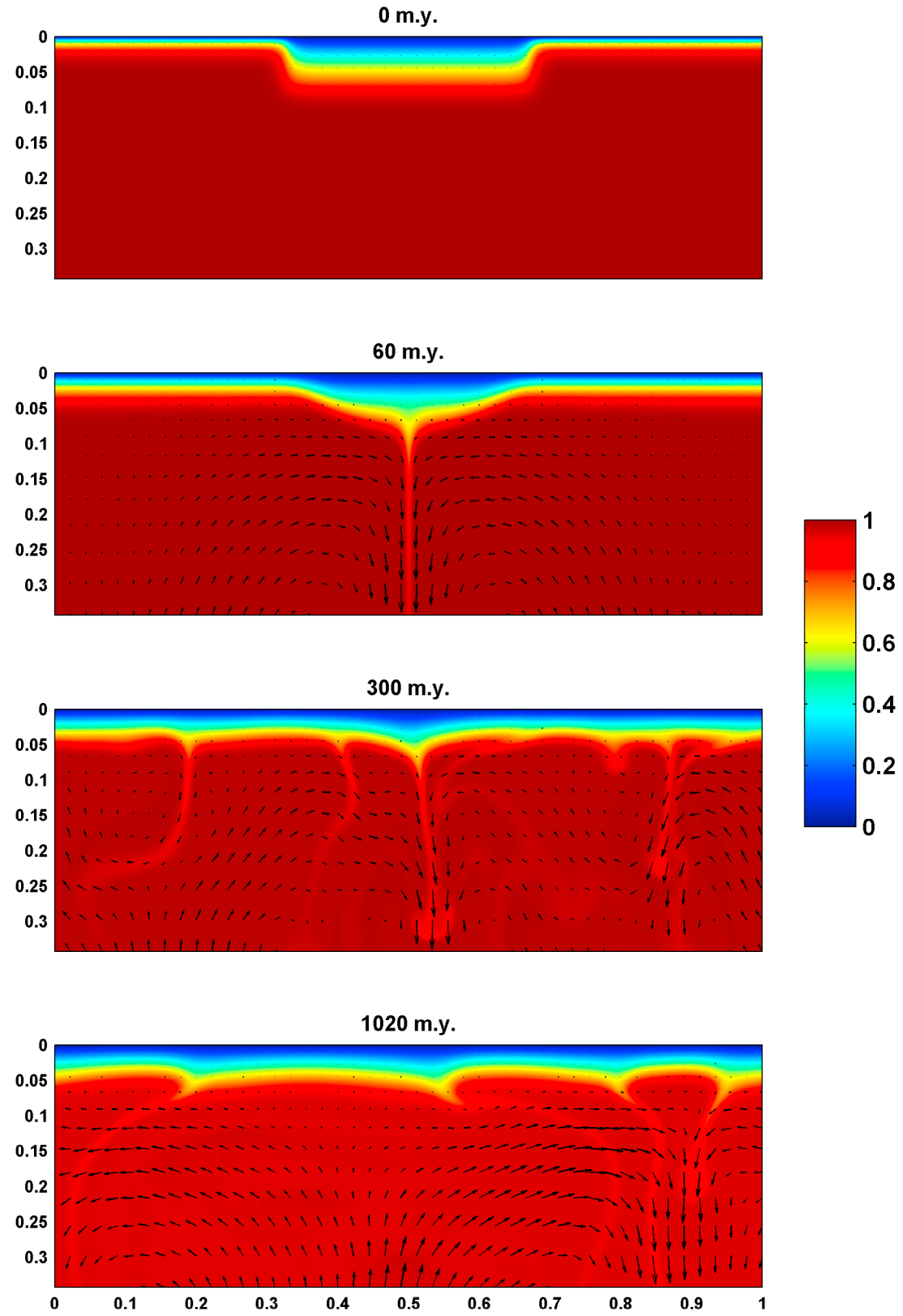

Figure 7. Temporal evolution of a mantle convection simulation with Rayleigh number $Ra = 10^9$ and viscosity ratio $\mu_r = 10^5$. Only the upper 1000 km of the whole mantle (2890 km) model are shown. The cratonic keel (defined by a cold temperature anomaly, see setup in Figure 2b) is readily eroded away on the order of 100 Myr by the turbulent convection in this relatively low viscosity ratio regime. The base of the thermal lithosphere exits the diamond stability for this low viscosity ratio simulation (red in Figure 9), indicating that for such viscosity ratio the cratonic keel is not stable.

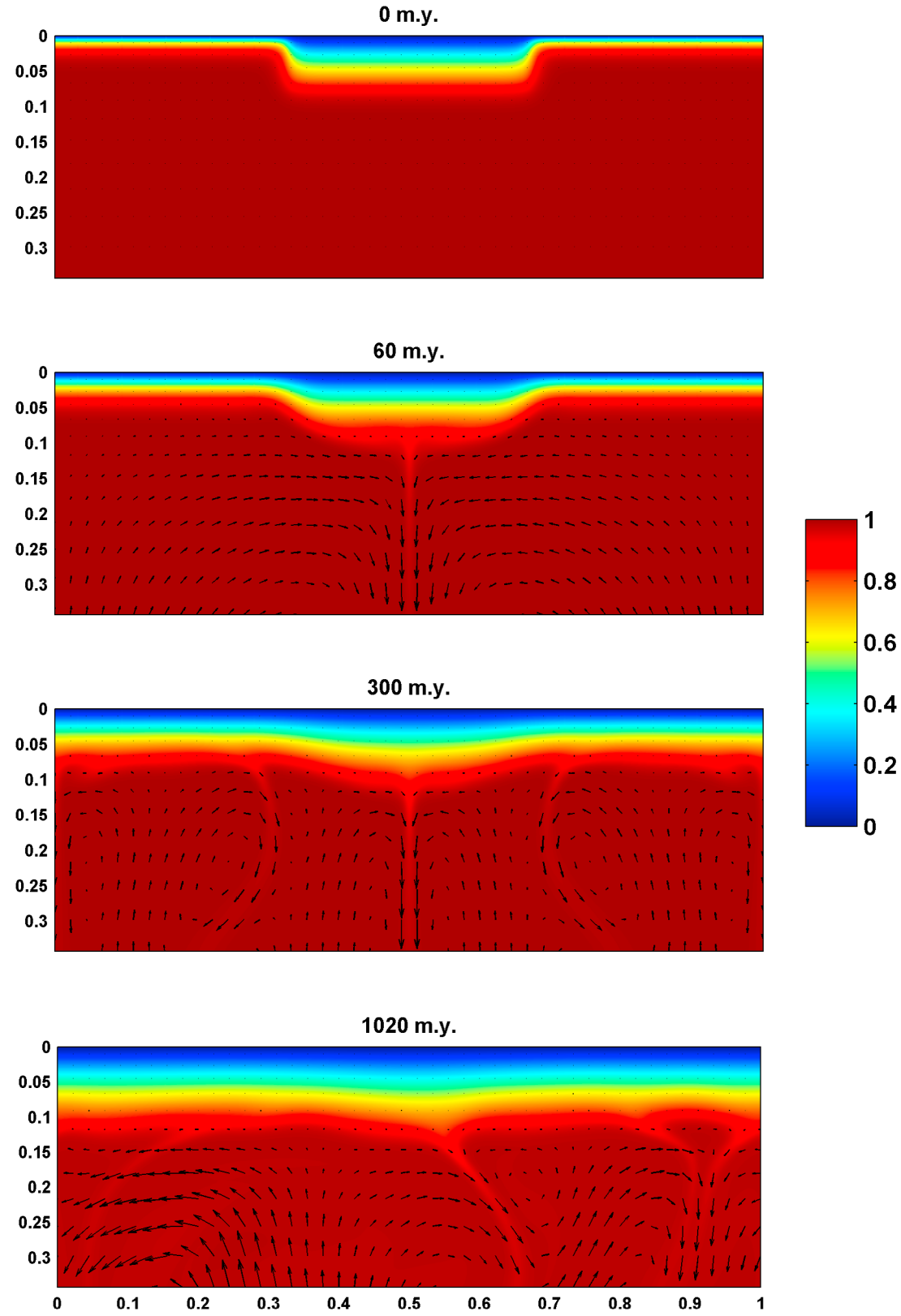

Figure 8. Temporal evolution of a mantle convection simulation with Rayleigh number $Ra = 10^9$ and viscosity ratio $\mu_r = 10^{10}$. The cratonic keel remains stable due to the high viscosity ratio throughout the entire simulation time of ~1 Gyr. The base of the thermal lithosphere remains within the diamond stability for this high viscosity ratio simulation (blue in Figure 9) throughout the entire simulation, indicating long-term stability of the cratonic keel.

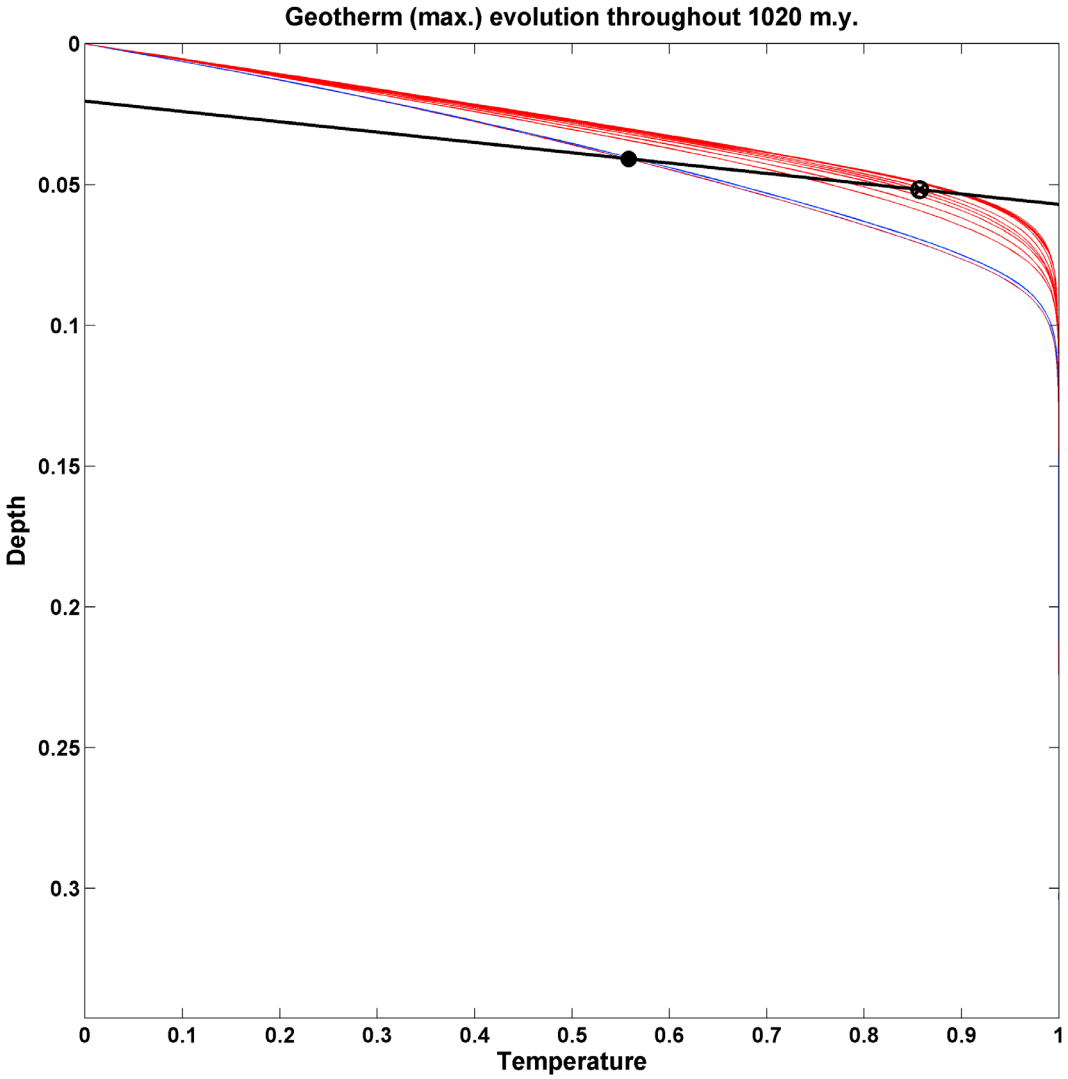

Figure 9. Mean geotherm below the craton for the highest temperatures recorded at intervals of 40 Myr for runs with low (red, $\mu_r = 10^5$) and high (blue, $\mu_r = 10^{10}$) viscosity ratios for the upper 1000 km of the mantle (corresponding to the part of the domain shown in Figures 7 and 8) at a bottom heating Rayleigh number $Ra = 10^9$. The total simulation time is ~1 Gyr. The black solid line shows the graphite-diamond transition (GDT) from *Kennedy and Kennedy* [1976]. The solid circle marks the intersection of the initial geotherm (equivalent for both runs) with the GDT, and the crossed open circle marks the intersection of the GDT with the nondimensional temperature at the base of the thermal lithosphere (see text for explanation). Our criterion for craton stability is that the base of the thermal lithosphere remains below the GDT throughout the entire simulation time. This is the case for the high viscosity ratio simulation (blue) but not for the low viscosity ratio run (red).

tectonic-like behavior [*Lenardic et al.*, 2000, 2003; *O'Neill and Moresi*, 2003; *O'Neill et al.*, 2008].

[42] Due to the rationale outlined in section 1.2, we restricted our study to the stagnant lid regime. A thick thermal boundary layer therefore develops to the side of the model craton after several hundred million years which is not consistent with Earth's plate tectonics regime. Still, during the initial phase (<100–200 Myr), our model exhibits, due to choice of the initial temperature condition, a strong lateral temperature gradient between oceanic and continental lithosphere which is comparable to the situation on Earth. The fact that during this first phase, the craton is rapidly eroded from the sides for low viscosity ratios, but preserves its initial width for the high viscosity ratios, indicates that the lateral preservation of the cratonic root is a function of the temperature-dependent viscosity ratio. Thus, high viscosity ratios can preserve cratons from erosion by downwelling at its sides even when strong lateral temperature gradients are present. Our observation that convective destabilization is primarily due to lateral temperature gradients between thick (cratonic) root and thin adjacent (oceanic) lithosphere agrees with the conclusion drawn by *Doin et al.* [1997] for their study of continental lithosphere stability, even though *Doin et al.* [1997] include plate tectonic features like oceanic lithosphere spreading and subducting slabs.

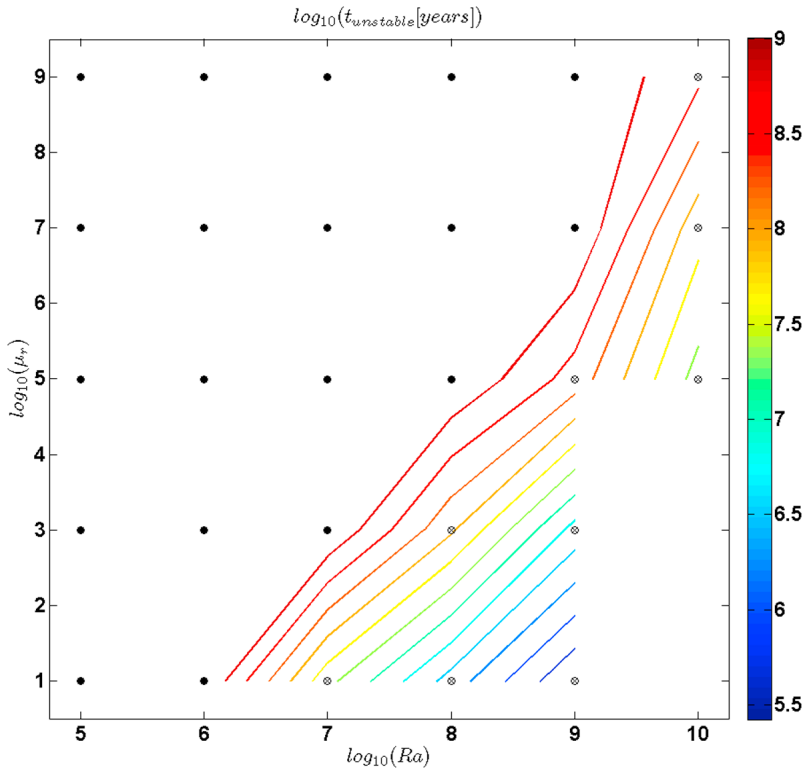

Figure 10. Explored range of Rayleigh numbers Ra and viscosity ratio μ_r and associated time to instability $t_{unstable}$ for the whole mantle setting (see Figure 6 for details). Simulations with $Ra = 10^{10}$ and viscosity ratios $\mu_r = 10$ and $\mu_r = 10^3$ could not be conducted due to numerical restrictions.

[43] If cratons are indeed thermally eroded in some models with plate tectonics [*O'Neill and Moresi*, 2003], they are, according to previous authors [*Lenardic and Moresi*, 1999; *Lenardic et al.*, 2003], expected to be relatively more stable in models that lack plate tectonics, i.e., in stagnant lid models like ours. When we compare our results for the same range of Rayleigh numbers and the same small temperature-dependent viscosity ratio of 10^5 as employed in previous studies with plate tectonics-like regime [*O'Neill and Moresi*, 2003] in the upper mantle setup, we find that the model craton is thermally unstable both in those previous plate tectonics simulations (for Rayleigh numbers 10^7–10^8) and in our stagnant lid simulations. This suggests that a temperature-dependent viscosity ratio of 10^5 is in both cases, i.e., with or without active surface tectonics, too small to provide for long-term craton stability. Since increasing the temperature-dependent viscosity ratio in our stagnant lid simulations had a strong stabilizing effect, it seems important to investigate the effect of larger temperature-dependent viscosity ratios on craton stability in future plate tectonics models.

4.2. Viscous or Viscoelastic Mantle Rheology?

[44] Even though mantle rocks are viscoelastic, it is common practice to model the mantle as a viscous fluid in geodynamic simulations. For the hot, convecting interior of our planet, stresses relax on the order of 10,000 years, as evidenced, e.g., from studies of postglacial rebound [*Haskell*, 1935]; thus, the assumption of a viscous fluid seems appropriate. Yet, when the cold, rigid lithosphere is included in simulations, stresses can be stored within the lithosphere over long geological times due to elasticity. The question arises whether elasticity plays a significant role in geodynamic simulations that include the lithosphere. For the problem of craton stability, we have shown that the dependence of the time to instability $t_{unstable}$ on Rayleigh number Ra, viscosity ratio μ_r and initial craton thickness z_c is very similar for viscous and viscoelastic rheologies. Apparently, elasticity within the lithosphere does not play a significant role for the problem of craton stability. Since the cratonic keel exhibits high viscosities and consequently lacks large-scale deformation, both viscous and viscoelastic rheologies produce a stable cratonic keel. Yet, as we discuss in section 4.3 and as demonstrated by *Beuchert and Podladchikov* [2010], viscoelasticity provides a physical transition from viscous to elastic behavior depending on the local magnitude of viscosity ratio and thus helps to avoid introduction of nonphysical viscosity cutoffs commonly applied in models with viscous rheology. Further, the stress distribution within the lithosphere differs significantly between viscous and viscoelastic simulations, an effect presented by *Beuchert and Podladchikov* [2010]. Future craton stability models that include stress-dependent processes like plastic yielding should thus also incorporate elasticity, since plastic yielding depends critically on the stress level inside the lithosphere.

4.3. Viscoelastic Transition in Viscoelastic Rheology

[45] The viscoelastic nature of rocks is most apparent when considering the different response of the mantle sub-

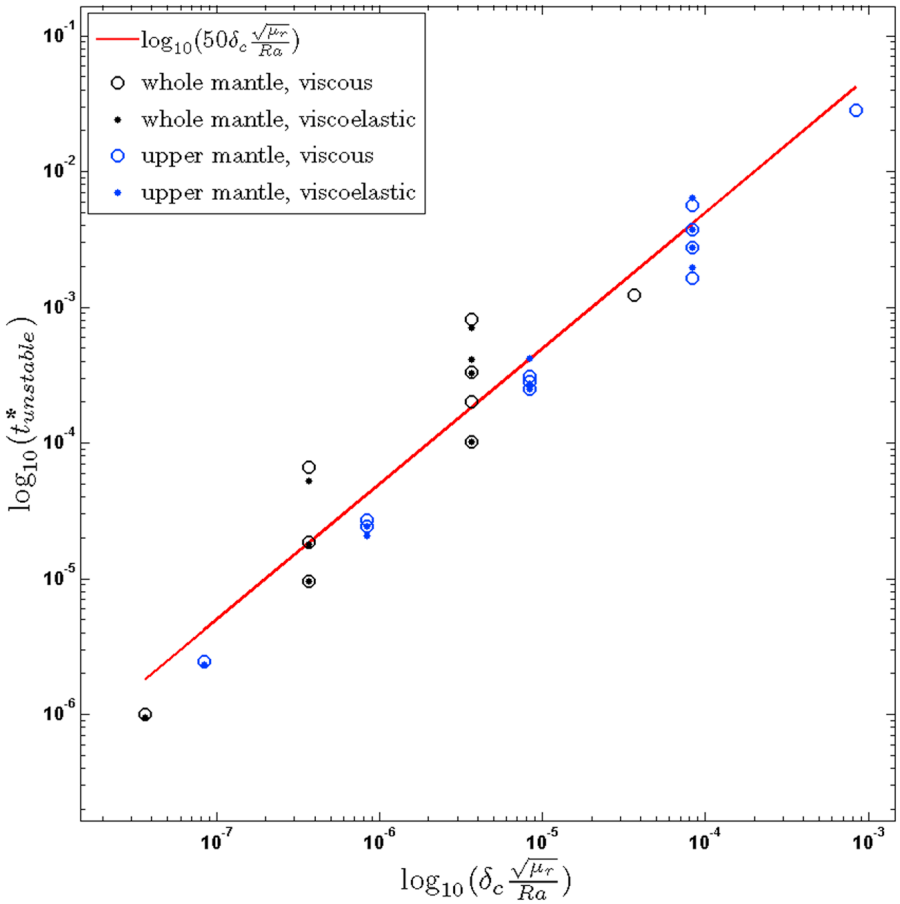

Figure 11. Data collapse for the results from upper (blue) and whole (black) mantle simulations as presented in Figures 6 and 10. The fit of the numerical results for the nondimensional time to craton instability $t_{unstable}$* yields the relation (19) (red line). This holds both for viscoelastic (points) and viscous (open circles) simulations.

jected to earthquake waves and thermal buoyancy forces. Earthquake waves travel through the mantle on time scales of seconds to hours. Due to the short loading time, the mantle responds elastically. In contrast, when subjected to loading on thousand to millions of years, the deep Earth interior flows in a viscous manner. Thus, the mantle can respond both as an elastic solid and as a viscous fluid, a behavior that can be captured by a Maxwell viscoelastic rheology. The constitutive equation for a Maxwell material was already given above and is restated here (equation (5)):

$$\dot{\varepsilon}'_{ij} = \underbrace{\frac{1}{2\mu(T)}\tau_{ij}}_{viscous} + \underbrace{\frac{1}{2G}\frac{\mathrm{D}\tau_{ij}}{\mathrm{D}t}}_{elastic}.$$

The constitutive equation (5) shows that apart from the time span dt under consideration as discussed above, the response of the mantle depends on two additional parameters: shear viscosity μ and elastic shear modulus G, which in (5) pertain to the viscous and elastic contribution to the bulk strain rate $\dot{\varepsilon}'_{ij}$, respectively. Since G varies only by about one order of magnitude throughout the depth of the mantle, the response is mostly a function of loading time and viscosity. For short loading times (seconds to hours), the response of the mantle will always be dominated by elasticity because of the generally high viscosity of the mantle. For long loading times (hundreds to billions of years), the response depends on the specific value of the shear viscosity μ in any given volume of the mantle. For the hot, sublithospheric mantle with moderate viscosities (10^{19}–10^{21} Pa s), the response is viscous already on a 10,000 year time scale, as evidenced, e.g., from postglacial rebound. It is this viscous response on long time scales that ultimately allows for the large-scale convective mantle flow. Cold, lithospheric mantle instead exhibits several orders of magnitude higher viscosities due to the strong temperature dependence of creep activation (compare section 1.3 and Figure 1). Thus, the elastic part in (5) dominates over the viscous part even on long geological times (more than hundreds of millions of years). This results in long-term elastic behavior of the lithosphere as indicated by large values of Maxwell relaxation time $t_{Maxwell}$ in the lithosphere (Figure 1d). Using viscosities of the sublithospheric mantle as obtained from studies of postglacial rebound (original work by *Haskell* [1935]), $t_{Maxwell}$ can be determined to be on the order of only thousands of years for the sublithospheric mantle; consequently, for timescales larger than this, the

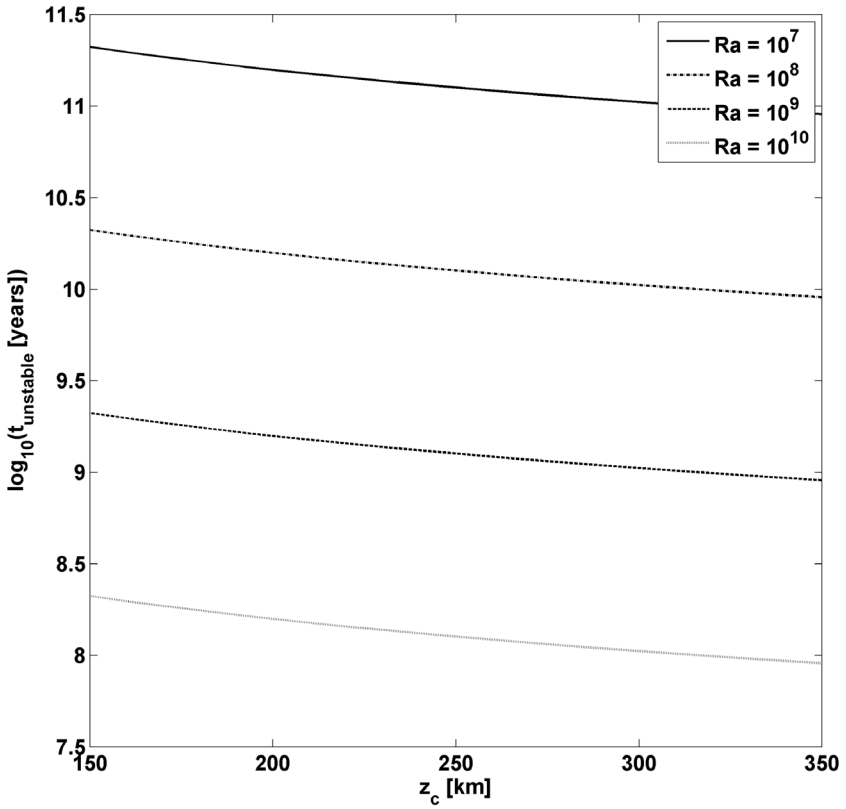

Figure 12. Dependence of the time to instability $t_{unstable}$ on the thickness of the initial model craton z_c according to (19) for a realistic viscosity ratio (see text for details) and a range of realistic Rayleigh numbers *Ra* for the whole mantle.

response of the sublithospheric mantle is dominantly viscous. Based on this observation, numerical mantle convection simulations commonly apply a viscous rheology for the entire mantle. For the sublithospheric mantle, this is a valid approach, but this assumption breaks down when the lithosphere, and in particular cold continental lithosphere, is included in the models. For cold lithospheric keels, viscosities are extremely high (see section 1.3, Figure 1b), resulting in Maxwell relaxation times $t_{Maxwell}$ on the order of billions of years (see Figure 1d). Hence, due to the inhibition of stress relaxation, the lithospheric keel is effectively in an elastic state and can preserve stresses for billions of years. The effectively elastic response of the cold lithosphere agrees with the "mechanical" definition of the lithosphere, i.e., the thickness of the rigid, elastically responding part of the mantle (see discussion by *Anderson* [1995]).

[46] Figure 13 shows a conceptual model of the rheological transition from viscous to elastic behavior of a viscoelastic model within a cratonic keel. At the base of the keel, the response of the mantle is dominantly viscous due to

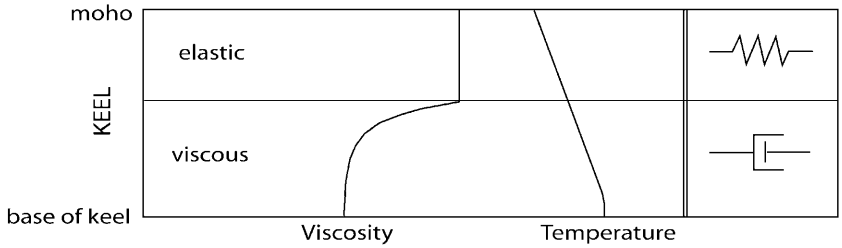

Figure 13. Schematic illustration of the transition from viscous to elastic behavior inside the lithospheric keel with decreasing depth due to the temperature dependence of viscosity. With decreasing temperature (schematic conductive keel geotherm shown), the viscosity in the lithosphere increases to very high values (see section 1.3 and Figure 1), resulting in elastic behavior of the mantle rocks in the upper part of the lithospheric keel. The pictograms (right) mark depth ranges of dominantly viscous (dashpot) and dominantly elastic behavior (spring). For high viscosities, the viscoelastic rheology becomes insensitive to further viscosity increases since the response is elastic.

the relatively low viscosities of the hot sublithospheric mantle. When entering the keel, the viscosities become, due to the strong temperature dependence of viscosity, so high that the rheological regime changes from viscously dominated to elastically dominated. Even though viscosities still increase in the upper part of the lithosphere, the viscoelastic model is insensitive to this increase, since the rheology is strongly dominated by elasticity.

[47] By providing a physical transition from viscous to elastic behavior depending on the local viscosity ratio, the viscoelastic rheology helps to avoid viscosity cutoffs commonly applied in geodynamic simulations with viscous rheology [e.g., *de Smet et al.*, 1999; *Doin et al.*, 1997; *Lenardic and Kaula*, 1996; *Ribe and Christensen*, 1994; *Shapiro et al.*, 1999]. The implications of the viscoelastic transition of a viscoelastic rheology for numerical modeling with large viscosity ratios are discussed elsewhere [*Beuchert and Podladchikov*, 2010].

4.4. Implications for the Role of Petrology in the Destruction of Cratonic Mantle

[48] As outlined in section 1, geochemical and petrological data from Archean mantle lithosphere is consistent with the preservation of cold cratons for billions of years. However, some cratons are destroyed and convincing evidence for delamination and rifting of cratons has been collected in several recent studies [e.g., *Carlson et al.*, 2004; *Tappe et al.*, 2007; *Zheng et al.*, 2007]. Since our study shows that the large temperature dependence of viscosity can provide for stability of cratons over billions of years in stagnant lid models without invoking the effect of strengthening due to chemical depletion and since this might also be the case for plate tectonics models with larger temperature-dependent viscosity ratio, the question arises why and how some cratonic keels are actually destroyed over time. Detailed field, petrological and geochemical studies indicate that large-scale destruction of cratons is preceded by episodic chemical rejuvenation of the lithospheric mantle. Based on these data, *Foley* [2008] developed a conceptual model that invokes the infiltration of small degree melts and fluids that react with the refractory mantle and form enriched and hydrated veins. These veins are characterized by lower solidus temperatures than the surrounding unmetasomatized peridotite and will preferentially melt during later thermal events. Over time these zones of melt impregnation might grow and coalesce, forming deep incisions at the craton base. In contrast to models invoking only the effect of transient thermal weakening, e.g., due to infiltration of hot melts, the change in physical properties due to changes in chemical composition and phase relations is permanent and may eventually lead to erosion of the lithospheric keel. In summary, compositional and mineralogical variations probably play an important role for craton stability. However, while the chemical processes are well documented by studies on mantle xenoliths and continental magmas and backed up by high pressure and temperature experiments (see review by *Foley* [2008]), quantitative studies on the relationship between chemical-petrological and thermomechanical processes are still in their infancy. *Li et al.* [2008] investigated the effect of metasomatic hydration on the strength of the lithosphere. Even though they only looked at the effect of water in nominally anhydrous minerals, they conclude that the weakening due to metasomatism is significant. *Neves et al.* [2008] have recently modeled the effect of regions with higher radiogenic heat production (which the rejuvenated areas described by Foley should be) on lithosphere dynamics. *Foley* [2008] stresses the changes of oxidation state related to the formation and remelting of metasomatic veins, which may also influence viscosity [*Dohmen et al.*, 2007].

[49] Hence, future models of lithosphere evolution should also consider coupling between thermomechanical and chemical processes such as partial melting, melt infiltration and changes in density and rheology due to melt impregnation.

5. Conclusions

[50] The relation (19) obtained from our stagnant lid simulations shows that the question whether cratons are stable over long geological times depends, for a given craton thickness, both on Rayleigh number and temperature-dependent viscosity ratio. If the viscosity ratio is fixed at a too low value or a too low viscosity cutoff is introduced, cratons do not remain stable over long geological times. Yet, laboratory experiments (section 1.3) indicate that realistic temperature-dependent viscosity ratios for the Earth's mantle are very high indeed, such that the limit for numerical modeling is only restricted by the ability of the code to handle large viscosity variations. Within the frame of stagnant lid convection, our numerical modeling results show that a large temperature-dependent viscosity ratio between cold cratonic lithosphere and the convecting mantle can provide for long-term stability of cratonic lithosphere even for realistically high Rayleigh numbers and without introducing compositionally increased viscosity of the craton. Whether large temperature-dependent viscosity ratios have a stabilizing effect in models with active surface tectonics remains to be explored. We suggest that a viscoelastic rheology provides a physical transition from viscous to elastic response for large local values of viscosity ratio, thereby rendering introduction of viscosity cutoffs unnecessary. Further, lithospheric stress distributions were found to be substantially different for simulations with viscous and viscoelastic rheology [*Beuchert and Podladchikov*, 2010], suggesting that future models that incorporate stress-dependent plastic yielding should apply a viscoelastic flow law.

Notation

$\dot{\varepsilon}$ shear strain rate (scalar), s^{-1}.
σ shear stress (scalar), Pa.
A preexponential factor, s^{-1}.
G elastic shear modulus, Pa.
b length of the Burgers vector, describing the crystal lattice spacing, m.
d grain size, m.
n stress exponent.
m grain size exponent.
E_a activation energy, J mol^{-1}.
p pressure, Pa.
V_a activation volume, m^3 mol^{-1}.

R universal gas constant, equal to 8.314472, J K^{-1} mol^{-1}.
T temperature, K.
T_0 maximum temperature in the domain, K.
ρ_0 density at reference temperature T_0, kg m^{-3}.
t time, s.
α thermal expansion coefficient, K^{-1}.
μ shear viscosity, Pa s.
μ_0 shear viscosity at reference temperature T_0, Pa s.
κ heat diffusivity, m^2 s^{-1}.
γ creep activation, K^{-1}.
h domain height, m.
ΔT temperature difference throughout the domain, K.
v_i velocity vector, m s^{-1}.
x_i Eulerian coordinates vector, m.
g acceleration of gravity, m s^{-2}.
$\hat{\mathbf{z}}$ unit vector pointing vertically downward.
σ_{ij} total stress tensor, Pa.
τ_{ij} deviatoric stress tensor, Pa.
$\dot{\varepsilon}_{ij}$ strain rate tensor, s^{-1}.
$\dot{\varepsilon}'_{ij}$ deviatoric strain rate tensor, s^{-1}.
ω_{ij} vorticity tensor, s^{-1}.
Ra Rayleigh number.
De Deborah number.
λ creep activation parameter.
μ_r viscosity ratio.
z_c thickness of model craton, m.
δ_c ratio of domain height to thickness of model craton.

[51] **Acknowledgments.** Marcus Beuchert was supported by research grant 163464 from the Norwegian Research Council. We would like to thank our colleagues at PGP for continuous discussions.

References

Anderson, D. L. (1995), Lithosphere, asthenosphere, and perisphere, *Rev. Geophys.*, *33*(1), 125–149, doi:10.1029/94RG02785.

Anderson, D. L., and J. D. Bass (1984), Mineralogy and composition of the upper mantle, *Geophys. Res. Lett.*, *11*(7), 637–640, doi:10.1029/GL011i007p00637.

Beuchert, M. J., and Y. Y. Podladchikov (2010), Viscoelastic mantle convection and lithospheric stresses, *Geophys. J. Int.*, *183*, 35–63, doi:10.1111/j.1365-246X.2010.04708.x.

Boyd, F. R., and P. H. Nixon (1975), Origins of the ultramafic nodules from some kimberlites of northern Lesotho and the Monastery Mine, South Africa, in *Proceeding of the First International Conference on Kimberlites, Cape Town, 1973*, edited by L. H. Ahrens et al., pp. 431–454, Pergamon, Oxford, U. K.

Boyd, F. R., J. J. Gurney, and S. H. Richardson (1985), Evidence for a 150–200-km thick Archean lithosphere from diamond inclusion thermobarometry, *Nature*, *315*(6018), 387–389, doi:10.1038/315387a0.

Bulanova, G. P. (1995), The formation of diamond, *J. Geochem. Explor.*, *53*(1–3), 1–23, doi:10.1016/0375-6742(94)00016-5.

Burov, E. B., and M. Diament (1995), The effective elastic thickness (T_e) of continental lithosphere: What does it really mean?, *J. Geophys. Res.*, *100*(B3), 3905–3927, doi:10.1029/94JB02770.

Burov, E., C. Jaupart, and J.C. Mareschal (1998), Large-scale crustal heterogeneities and lithospheric strength in cratons, *Earth Planet. Sci. Lett.*, *164*(1–2), 205–219, doi:10.1016/S0012-821X(98)00205-2.

Carlson, R. W., et al. (1999), Re-Os systematics of lithospheric peridotites: Implications for lithosphere formation and preservation, in *Proceedings of the 7th International Kimberlite Conference, Cape Town, 1998*, edited by J. J. Gurney et al., pp. 99–108, Red Roof Design, Cape Town, South Africa.

Carlson, R. W., A. J. Irving, D. J. Schulze, and B. C. Hearn Jr. (2004), Timing of Precambrian melt depletion and Phanerozoic refertilization events in the lithospheric mantle of the Wyoming Craton and adjacent Central Plains Orogen, *Lithos*, *77*(1–4), 453–472, doi:10.1016/j.lithos.2004.03.030.

Cooper, C. M., A. Lenardic, and L. Moresi (2004), The thermal structure of stable continental lithosphere within a dynamic mantle, *Earth Planet. Sci. Lett.*, *222*(3–4), 807–817, doi:10.1016/j.epsl.2004.04.008.

Cooper, C. M., et al. (2006), Creation and preservation of cratonic lithosphere; seismic constraints and geodynamic models: Archean geodynamics and environments, in *Archean Geodynamics and Environments*, *Geophys. Monogr. Ser.*, vol. 164, edited by K. Benn, J.-C. Mareschal, and K. C. Condie, pp. 75–88, AGU, Washington, D. C.

de Smet, J. H., A. P. van den Berg, and N. J. Vlaar (1999), The evolution of continental roots in numerical thermo-chemical mantle convection models including differentiation by partial melting, *Lithos*, *48*, 153–170, doi:10.1016/S0024-4937(99)00028-6.

de Smet, J. H., A. P. Van den Berg, and N. J. Vlaar (2000), Early formation and long-term stability of continents resulting from decompression melting in a convecting mantle, *Tectonophysics*, *322*, 19–33, doi:10.1016/S0040-1951(00)00055-X.

Dohmen, R., H.-W. Becker and S. Chakraborty (2007), Fe-Mg diffusion in olivine I: Experimental determination between 700 and 1,200°C as a function of composition, crystal orientation and oxygen fugacity, *Phys. Chem. Miner.*, *34*(6), 389–407, doi:10.1007/s00269-007-0157-7.

Doin, M.-P., L. Fleitout, and U. Christensen (1997), Mantle convection and stability of depleted and undepleted continental lithosphere, *J. Geophys. Res.*, *102*(B2), 2771–2787, doi:10.1029/96JB03271.

Finnerty, A. A., and F. R. Boyd (1987), Thermobarometry for garnet peridotites: Basis for the determination of thermal and compositional structure of the upper mantle, in *Mantle Xenoliths*, edited by P. H. Nixon, pp. 381–402, John Wiley, Chichester, U. K.

Foley, S. F. (2008), Rejuvenation and erosion of the cratonic lithosphere, *Nat. Geosci.*, *1*(8), 503–510, doi:10.1038/ngeo261.

Garfunkel, Z. (2007), Controls of stable continental lithospheric thickness: The role of basal drag, *Lithos*, *96*(1–2), 299–314, doi:10.1016/j.lithos.2006.09.014.

Grand, S. P. (2002), Mantle shear-wave tomography and the fate of subducted slabs, *Philos. Trans. R. Soc. A*, *360*, 2475–2491, doi:10.1098/rsta.2002.1077.

Griffin, W. L., et al. (1999), The composition and origin of sub-continental lithospheric mantle, in *Mantle Petrology: Field Observations and High Pressure Experimentation: A Tribute to Francis R. (Joe) Boyd*, edited by Y. Fei et al., *Spec. Publ. Geochem. Soc.*, *6*, 13–45.

Griffin, W. L., S. Y. O'Reilly, N. Abe, S. Aulbach, R. M. Davies, N. J. Pearson, B. J. Doyle, and K. Kivi (2003), The origin and evolution of Archean lithospheric mantle, *Precambrian Res.*, *127*, 19–41, doi:10.1016/S0301-9268(03)00180-3.

Gu, Y. J., A. M. Dziewonski, W. Su, and G. Ekström (2001), Models of the mantle shear velocity and discontinuities in the pattern of lateral heterogeneities, *J. Geophys. Res.*, *106*, 11,169–11,199, doi:10.1029/2001JB000340.

Gurnis, M., et al. (Eds.) (1998), *The Core-Mantle Boundary Region*, *Geodyn. Ser.*, vol. 28, 334 pp., AGU, Washington, D. C.

Haskell, N. A. (1935), The motion of a viscous fluid under a surface load, *Physics*, *6*(8), 265–269, doi:10.1063/1.1745329.

Janse, A. J. A., and P. A. Sheahan (1995), Catalogue of world wide diamond and kimberlite occurrences: A selective and annotative approach, *J. Geochem. Explor.*, *53*(1–3), 73–111, doi:10.1016/0375-6742(94)00017-6.

Jaupart, C., and J. C. Mareschal (1999), The thermal structure and thickness of continental roots, *Lithos*, *48*(1–4), 93–114, doi:10.1016/S0024-4937(99)00023-7.

Jordan, T. H. (1978), Composition and development of the continental tectosphere, *Nature*, *274*(5671), 544–548, doi:10.1038/274544a0.

Karato, S., and P. Wu (1993), Rheology of the upper mantle—A synthesis, *Science*, *260*(5109), 771–778, doi:10.1126/science.260.5109.771.

Kennedy, C. S., and G. C. Kennedy (1976), Equilibrium boundary between graphite and diamond, *J. Geophys. Res.*, *81*(14), 2467–2470, doi:10.1029/JB081i014p02467.

King, S. D. (2005), Archean cratons and mantle dynamics, *Earth Planet. Sci. Lett.*, *234*(1–2), 1–14, doi:10.1016/j.epsl.2005.03.007.

King, S. D., and J. Ritsema (2000), African hot spot volcanism: Small-scale convection in the upper mantle beneath cratons, *Science*, *290*(5494), 1137–1140, doi:10.1126/science.290.5494.1137.

Kramers, J. D. (1979), Lead, uranium, strontium, potassium and rubidium in inclusion-bearing diamonds and mantle-derived xenoliths from southern Africa, *Earth Planet. Sci. Lett.*, *42*(1), 58–70, doi:10.1016/0012-821X(79)90190-0.

Kramers, J. D., J. C. M. Roddick, and J. B. Dawson (1983), Trace element and isotope studies on veined, metasomatic and "MARID" xenoliths from Bultfontein, South Africa, *Earth Planet. Sci. Lett.*, *65*, 90–106, doi:10.1016/0012-821X(83)90192-9.

Lenardic, A., and W. M. Kaula (1996), Near surface thermal/chemical boundary layer convection at infinite Prandtl number: Two-dimensional numerical experiments, *Geophys. J. Int.*, *126*(3), 689–711.

Lenardic, A., and L. N. Moresi (1999), Some thoughts on the stability of cratonic lithosphere; effects of buoyancy and viscosity, *J. Geophys. Res.*, *104*(B6), 12,747–12,758, doi:10.1029/1999JB900035.

Lenardic, A., L. Moresi, and H. Mühlhaus (2000), The role of mobile belts for the longevity of deep cratonic lithosphere: The Crumple Zone Model, *Geophys. Res. Lett.*, *27*(8), 1235–1238, doi:10.1029/1999GL008410.

Lenardic, A., L.-N. Moresi, and H. Mühlhaus (2003), Longevity and stability of cratonic lithosphere: Insights from numerical simulations of coupled mantle convection and continental tectonics, *J. Geophys. Res.*, *108*(B6), 2303, doi:10.1029/2002JB001859.

Levinson, A. A., et al. (1992), Diamond sources and production: Past, present, and future, *Gems Gemol.*, *28*(4), 234–254.

Li, Z.-X. A., C.-T. A. Lee, A. H. Peslier, A. Lenardic, and S. J. Mackwell (2008), Water contents in mantle xenoliths from the Colorado Plateau and vicinity: Implications for the mantle rheology and hydration-induced thinning of continental lithosphere, *J. Geophys. Res.*, *113*, B09210, doi:10.1029/2007JB005540.

Lowrie, W. (2007), *Fundamentals of Geophysics*, 2nd ed., 381 pp., Cambridge Univ. Press, Cambridge, U. K.

MacGregor, I. D. (1975), Petrologic and thermal structure of the upper mantle beneath South Africa in the Cretaceous, *Phys. Chem. Earth*, *9*, 455–466, doi:10.1016/0079-1946(75)90033-6.

Malkovets, V. G., W. L. Griffin, S. Y. O'Reilly, and B. J. Wood (2007), Diamond, subcalcic garnet, and mantle metasomatism: Kimberlite sampling patterns define the link, *Geology*, *35*, 339–342, doi:10.1130/G23092A.1.

Menzies, M., and V. Murthy (1980), Enriched mantle: Nd and Sr isotopes in diopsides from kimberlite nodules, *Nature*, *283*, 634–636, doi:10.1038/283634a0.

Michaut, C., and C. Jaupart (2007), Secular cooling and thermal structure of continental lithosphere, *Earth Planet. Sci. Lett.*, *257*(1–2), 83–96, doi:10.1016/j.epsl.2007.02.019.

Montelli, R., G. Nolet, F. A. Dahlen, G. Masters, E. R. Engdahl, S.-H.Hung (2004), Finite-frequency tomography reveals a variety of plumes in the mantle, *Science*, *303*(5656), 338–343, doi:10.1126/science.1092485.

Morelli, A., and A. M. Dziewonski (1987), Topography of the core-mantle boundary and lateral homogeneity of the liquid core, *Nature*, *325*(6106), 678–683, doi:10.1038/325678a0.

Moresi, L., and V. Solomatov (1998), Mantle convection with a brittle lithosphere; Thoughts on the global tectonic styles of the Earth and Venus, *Geophys. J. Int.*, *133*(3), 669–682, doi:10.1046/j.1365-246X.1998.00521.x.

Navon, O. (1999), Diamond formation in the Earth's mantle, in *Proceedings of the 7th International Kimberlite Conference*, edited by J. J. Gurney et al., pp. 584–604, Red Roof Design, Cape Town.

Neves, S. P., A. Tommasi, A. Vauchez, and R. Hassani (2008), Intraplate continental deformation: Influence of a heat-producing layer in the lithospheric mantle, *Earth Planet. Sci. Lett.*, *274*(3–4), 392–400, doi:10.1016/j.epsl.2008.07.040.

O'Neill, C. J., and L. N. Moresi (2003), How long can diamonds remain stable in the continental lithosphere?, *Earth Planet. Sci. Lett.*, *213*(1–2), 43–52, doi:10.1016/S0012-821X(03)00294-2.

O'Neill, C. J., A. Lenardic, W. L. Griffin, and S. Y. O'Reilly (2008), Dynamics of cratons in an evolving mantle, *Lithos*, *102*(1–2), 12–24, doi:10.1016/j.lithos.2007.04.006.

O'Reilly, S. Y., and W. L. Griffin (1996), 4-D lithosphere mapping: Methodology and examples, *Tectonophysics*, *262*(1–4), 3–18, doi:10.1016/0040-1951(96)00010-8.

O'Reilly, S. Y., and W. L. Griffin (2006), Imaging global chemical and thermal heterogeneity in the subcontinental lithospheric mantle with garnets and xenoliths: Geophysical implications, *Tectonophysics*, *416*(1–4), 289–309, doi:10.1016/j.tecto.2005.11.014.

Pearson, D. G., et al. (2002), The development of lithospheric keels beneath the earliest continents: Time constraints using PGE and Re-Os isotope systematics, in *The Early Earth: Physical, Chemical and Biological Development*, edited by C. M. R. Fowler et al., *Geol. Soc. Spec. Publ.*, *199*, 65–90.

Polet, J., and D. L. Anderson (1995), Depth extent of cratons as inferred from tomographic studies, *Geology*, *23*(3), 205–208, doi:10.1130/0091-7613(1995)023<0205:DEOCAI>2.3.CO;2.

Pollack, H., and D. Chapman (1977), On the regional variation of heat flow, geotherms, and lithospheric thickness, *Tectonophysics*, *38*, 279–296, doi:10.1016/0040-1951(77)90215-3.

Reiner, M. (1964), The Deborah number, *Phys. Today*, *17*(1), 62, doi:10.1063/1.3051374.

Ribe, N. M., and U. R. Christensen (1994), Three-dimensional modeling of plume-lithosphere interaction, *J. Geophys. Res.*, *99*(B1), 669–682, doi:10.1029/93JB02386.

Richardson, S. H., and J. W. Harris (1997), Antiquity of peridotitic diamonds from the Siberian craton, *Earth Planet. Sci. Lett.*, *151*(3–4), 271–277, doi:10.1016/S0012-821X(97)81853-5.

Richardson, S. H., J. J. Gurney, A. J. Erlank, and J. W. Harris (1984), Origin of diamonds in old enriched mantle, *Nature*, *310*, 198–202, doi:10.1038/310198a0.

Richardson, S. H., A. J. Erlank, J. W. Harris, and S. R. Hart (1990), Eclogitic diamonds of Proterozoic age from Cretaceous kimberlites, *Nature*, *346*, 54–56, doi:10.1038/346054a0.

Richardson, S. H., J. W. Harris, and J. J Gurney (1993), Three generations of diamonds from old continental mantle, *Nature*, *366*(6452), 256–258, doi:10.1038/366256a0.

Richardson, S. H., S. B. Shirey, J. W. Harris, and R. W. Carlson (2001), Archean subduction recorded by Re-Os isotopes in eclogitic sulfide inclusions in Kimberley diamonds, *Earth Planet. Sci. Lett.*, *191*(3–4), 257–266, doi:10.1016/S0012-821X(01)00419-8.

Richardson, S. H., S. B. Shirey, and J. W. Harris (2004), Episodic diamond genesis at Jwaneng, Botswana, and implications for Kaapvaal craton evolution, *Lithos*, *77*(1–4), 143–154, doi:10.1016/j.lithos.2004.04.027.

Ritsema, J., and R. M. Allen (2003), The elusive mantle plume, *Earth Planet. Sci. Lett.*, *207*(1–4), 1–12, doi:10.1016/S0012-821X(02)01093-2.

Ritsema, J., and H. van Heijst (2000), New seismic model of the upper mantle beneath Africa, *Geology*, *28*(1), 63–66, doi:10.1130/0091-7613(2000)28<63:NSMOTU>2.0.CO;2.

Ritsema, J., H. J. van Heijst, and J. H. Woodhouse (2004), Global transition zone tomography, *J. Geophys. Res.*, *109*, B02302, doi:10.1029/2003JB002610.

Rudnick, D. L., and A. A. Nyblade (1999), The thickness and heat production of Archean lithosphere: Constraints from xenolith thermobarometry and surface heat flow, in *Mantle Petrology: Field Observations and High Pressure Experimentation: A Tribute to Francis R. (Joe) Boyd*, edited by Y. Fei et al., *Spec. Publ. Geochem. Soc.*, *6*, 3–12.

Rudnick, R. L., C. S. Eldridge, and G. P. Bulanova (1993), Diamond growth history from in situ measurement of Pb and S isotopic compositions of sulfide inclusions, *Geology*, *21*(1), 13–16, doi:10.1130/0091-7613(1993)021<0013:DGHFIS>2.3.CO;2.

Shapiro, S. S., B. H. Hager, and T. H. Jordan (1999), Stability and dynamics of the continental tectosphere, *Lithos*, *48*, 115–133, doi:10.1016/S0024-4937(99)00025-0.

Simon, N. S. C., B. H. Hager, and T. H. Jordan (2007), The origin and evolution of the Kaapvaal cratonic lithospheric mantle, *J. Petrol.*, *48*(3), 589–625, doi:10.1093/petrology/egl074.

Sleep, N. H. (2003), Survival of Archean cratonal lithosphere, *J. Geophys. Res.*, *108*(B6), 2302, doi:10.1029/2001JB000169.

Solomatov, V. S., and L. N. Moresi (1996), Stagnant lid convection on Venus, *J. Geophys. Res.*, *101*(E2), 4737–4753, doi:10.1029/95JE03361.

Solomatov, V. S., and L. N. Moresi (2000), Scaling of time-dependent stagnant lid convection: Application to small-scale convection on Earth and other terrestrial planets, *J. Geophys. Res.*, *105*(B9), 21,795–21,817, doi:10.1029/2000JB900197.

Spetsius, Z. V., E. A. Belousov, W. L. Griffin, S. Y. O'Reilly, and N. J. Pearson (2002), Archean sulfide inclusions in Paleozoic zircon megacrysts from the Mir kimberlite, Yakutia: Implications for the dating of diamonds, *Earth Planet. Sci. Lett.*, *199*(1–2), 111–126, doi:10.1016/S0012-821X(02)00539-3.

Tappe, S., S. F. Foley, A. Stracke, R. L. Romer, B. A. Kjarsgaard, L. M. Heaman, and N. Joyce (2007), Craton reactivation on the Labrador Sea margins: $^{40}Ar/^{39}Ar$ age and Sr–Nd–Hf–Pb isotope constraints from alkaline and carbonatite intrusives, *Earth Planet. Sci. Lett.*, *256*(3–4), 433–454, doi:10.1016/j.epsl.2007.01.036.

van der Hilst, R. (1995), Complex morphology of subducted lithosphere in the mantle beneath the Tonga trench, *Nature*, *374*(6518), 154–157, doi:10.1038/374154a0.

van der Hilst, R. D., S. Widiyantoro, and E. R. Engdahl (1997), Evidence for deep mantle circulation from global tomography, *Nature*, *386*(6625), 578–584, doi:10.1038/386578a0.

Walker, R. J., R. W. Carlson, S. B Shirey, and F. R. Boyd (1989), Os, Sr, Nd, and Pb isotope systematics of southern African peridotite xenoliths: Implications for the chemical evolution of subcontinental mantle, *Geochim. Cosmochim. Acta*, *53*, 1583–1595, doi:10.1016/0016-7037(89)90240-8.

Watts, A. B. (1992), The effective elastic thickness of the lithosphere and the evolution of foreland basins, *Basin Res.*, *4*, 169–178, doi:10.1111/j.1365-2117.1992.tb00043.x.

Watts, A. B., and S. Zhong (2000), Observations of flexure and the rheology of oceanic lithosphere, *Geophys. J. Int.*, *142*(3), 855–875, doi:10.1046/j.1365-246x.2000.00189.x.

Westerlund, K., S. B. Shirey, S. H. Richardson, R. W. Carlson, J. J. Gurney, and J. W. Harris (2006), A subduction wedge origin for Paleoarchean peridotitic diamonds and harzburgites from the Panda kimberlite, Slave craton: Evidence from Re–Os isotope systematics, *Contrib. Mineral. Petrol.*, *152*(3), 275–294, doi:10.1007/s00410-006-0101-8.

Zheng, J. P., W. L. Griffin, S. Y. O'Reilly, C. M. Yu, H. F. Zhang, N. Pearson, and M. Zhang (2007), Mechanism and timing of lithospheric modification and replacement beneath the eastern North China Craton: Peridotitic xenoliths from the 100 Ma Fuxin basalts and a regional synthesis, *Geochim. Cosmochim. Acta*, *71*(21), 5203–5225, doi:10.1016/j.gca.2007.07.028.

M. J. Beuchert, Institut für Geowissenschaften, Facheinheit Geophysik, Goethe-Universität Frankfurt, Altenhöferallee 1, D-60438 Frankfurt am Main, Germany. (beuchert@geophysik.uni-frankfurt.de)

Y. Y. Podladchikov and N. S. C. Simon, Physics of Geological Processes, University of Oslo, PO Box 1048 Blindern, N-0316 Oslo, Norway.

L. H. Rüpke, Future Ocean, IFM-GEOMAR, Wischhofstr. 1-3, D-24148 Kiel, Germany.